ROBERT ALEXANDER MÜLLER

RADIATIVE RECOMBINATION IN THE PRESENCE OF AN INTENSE LASER FIELD

RADIATIVE RECOMBINATION IN THE PRESENCE OF AN INTENSE LASER FIELD

seit 1558

Friedrich-Schiller-Universität Jena
Physikalisch-Astronomische Fakultät
Helmholtz-Institut Jena

MASTERARBEIT

zur Erlangung des Grades eines

MASTER OF SCIENCE

vorgelegt von

ROBERT ALEXANDER MÜLLER

geboren in Darmstadt

September 2015, Jena

Robert Alexander Müller:
Radiative Recombination in the presence of an intense laser field

SUPERVISORS:
PD Dr. Andrey Surzhykov
Prof. Dr. Stephan Fritzsche

DECLARATIONS

EIGENSTÄNDIGKEITSERKLÄRUNG

Der Autor erklärt, die vorliegende Arbeit selbstständig und ohne Benutzung anderer als der angegebenen Hilfsmittel verfasst zu haben. Die aus fremden Quellen direkt oder indirekt übernommenen Gedanken sind ausnahmslos als solche kenntlich gemacht. Die Arbeit ist in gleicher oder ähnlicher Form oder auszugsweise noch nicht im Rahmen einer anderen Prüfung vorgelegt worden.

Jena, September 2015

Robert Alexander Müller

BIBLIOTHEKSERKLÄRUNG

Seitens des Autors bestehen keine Einwände, die vorliegende Masterarbeit für die öffentliche Nutzung in der Thüringer Universitäts- und Landesbibliothek zur Verfügung zu stellen.

Jena, September 2015

Robert Alexander Müller

It is not down in any map; true places never are.
— Herman Melville (Moby-Dick)

ABSTRACT

In this thesis we present a theoretical study on the radiative recombination of electrons into the ground state of hydrogen like ions in the presence of an intense external laser field. We employ for the description of this process Heisenberg's S-matrix theory, where the final bound state of the electron is constructed using first order time dependent perturbation theory. Two different initial electron states are considered. First asymptotically plane-wave-like electrons with a separable Coulomb-Volkov continuum wave function and secondly twisted electrons with a well defined orbital angular momentum constructed from Volkov states. Using this approach we perform detailed calculations for the angle-differential and total cross section of laser assisted radiative recombination considering low-Z ions and laser intensities in the range from $I_L = 10^{11}\,\mathrm{W/cm^2}$ to $I_L = 10^{13}\,\mathrm{W/cm^2}$. Special emphasis is put on the effects arising due to the laser dressing of the residual bound state. It is seen that the bound state dressing remarkably affects the total cross section and manifests moreover as asymmetries in the angular and energy distribution of the emitted photons. For incident Coulomb-Volkov electrons we study moreover the polarization of the emitted recombination radiation. Here we find that the direction of polarization is rotated depending on the energy of the emitted recombination photons.

ZUSAMMENFASSUNG

Die vorliegende Arbeit befasst sich mit dem Prozess der strahlenden Rekombination in starken Laserfeldern unter Beteiligung von wasserstoffähnlichen Ionen. Für die Beschreibung dieses Prozesses nutzen wir Heisenbergs S-Matrix Theorie. Die Wellenfunktion des gebundenen Endzustandes wird mit Hilfe von zeitabhängiger Störungstheorie in erster Ordnung konstruiert. Für den Eingangszustand ziehen wir zwei verschiedene Möglichkeiten in Betracht. Erstens separable Coulomb-Volkov Wellenfunktionen, welche räumlich asymptotisch einer ebenen Wellen entsprechen und zweitens Vortexelektronen mit einem wohldefinierten Bahndrehimpuls. Letztere konstruieren wir als Überlagerung von Volkov-Lösungen der zeitabhängigen Schrödingergleichung. Mit Hilfe dieser Herangehensweise berechnen wir den winkeldifferentiellen und totalen Wirkungsquerschnitt der lasergetriebenen Rekombination. Hierbei betrachten wir wasserstoffähnliche Ionen mit niedrigen Kernladungszahlen und Laserintensitäten von $I_L = 10^{11}\,\mathrm{W/cm^2}$ bis $I_L = 10^{13}\,\mathrm{W/cm^2}$. Im speziellen untersuchen wir die Effekte, welche von den laserinduzierten Veränderungen des gebundenen Endzustands herrühren. Unsere Ergebnisse zeigen, dass diese Veränderungen starken Einfluss auf den totalen Wirkungsquerschnitt haben und außerdem als Asymmetrien in der Winkel- und Energieverteilung der emittierten Photonen sichtbar werden. Für Coulomb-Volkov Elektronen als Eingangszustand berechnen wir darüber hinaus die Polarisation der emittierten Strahlung. Diese ändert die Richtung ihrer Polarisation abhängig von der Energie der ausgestrahlten Photonen.

CONTENTS

1 INTRODUCTION

The capture of an electron into a bound state of an atom or ion if accompanied by the emission of a photon is called *radiative recombination* (RR). This fundamental capture process can be observed for example in astrophysical and laboratory plasmas [1–3] and has been studied extensively both in theory and experiment already for decades (see Ref. [2, 4, 5] and references therein). If the electron and the nucleus it recombines with are exposed to an external laser field one speaks of *laser assisted radiative recombination* (LARR). In this case, which we sketched in Fig. 1.1, the characteristics of the emitted recombination radiation as well as the cross section of the process may change remarkably compared to RR. The energy distribution of the emitted recombination photons, for example, is possibly broadened due to an acceleration or deceleration of the incident electron in the laser field. This modification of the recombination spectrum allows for the interpretation of LARR as the third step in the process of high harmonic generation [6, 7]. In addition laser assisted recombination processes have gained rising interest because the external laser can cause a significant increase of the recombination yield and therefore may support the creation of neutral antimatter [8–10].

There have been a number of experiments investigating LARR e.g. at the test storage ring (TSR) in Heidelberg, at the GSI in Darmstadt and at the Helmhotz-Institute Jena [11–15]. To support the findings of these experiments and make predictions for further investigations several theoretical studies have been performed [6, 7, 16–18]. In particular a theory based on the so called *strong field approximation* (SFA) has been developed by Keldysh, Faisal and Reiss and has been widely used up to now [16–18]. In this approximation the influence of the atomic nucleus on the incident electrons is neglected and it is assumed moreover that the residual bound state is unaltered by the external laser. During the recent years the SFA-based description of LARR has been improved. In a first attempt the influence of the nucleus on the incident electron state has been included in an approximate way [19]. More recently a theory has been developed that describes the residual bound state accounting for both the atomic and the laser potential either perturbatively or by means of a Floquet expansion [20–24].

In this thesis we aim to give a detailed characterization of LARR using a theory that is based on the extended SFA approaches used by Li *et al.* [21] as well as Shchedrin *et al.* [22]. In their works Li and Shchedrin presented only rough estima-

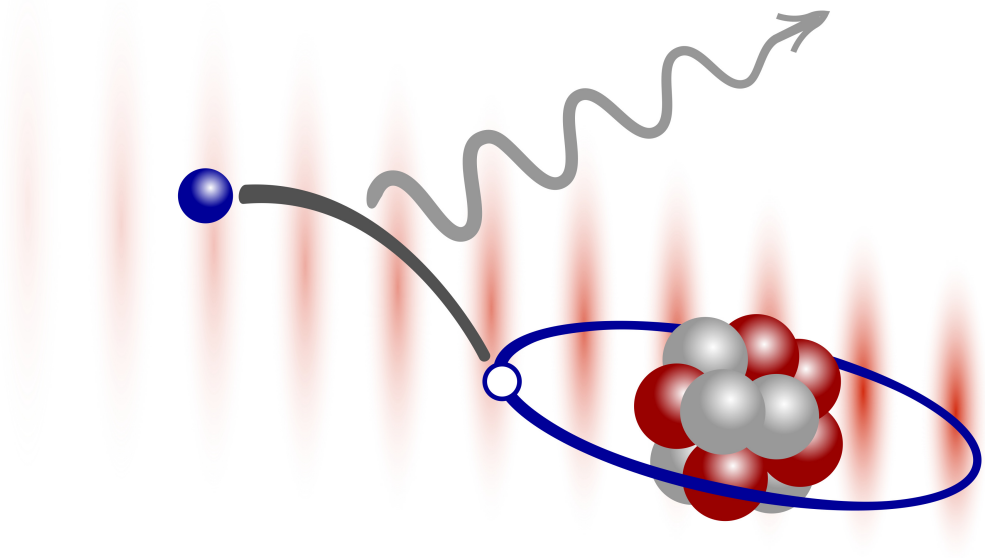

Figure 1.1: Sketch of the process of laser assisted radiative recombination. A continuum electron moving in the combined potential of an external laser and its parent nucleus is captured into a bound state of an atom or ion accompanied by the emission of a photon.

tions for the total cross section of LARR and a few numerical calculations. We aim to extend these attempts in the present work and moreover explain analytically as well as numerically how the external laser and especially its interaction with the residual bound state influences the angle-differential and total cross section of LARR. To the author's knowledge this has not been discussed in the context of LARR yet, however similar considerations have been made for two-color photoionization [25]. Furthermore we are interested in the polarization of the recombination photons emitted by means of LARR. While in laser free RR the emitted radiation is completely linear polarized, it has been shown that this behaviour might be modified if the process happens in presence of an external laser [20]. Therefore we will perform a comprehensive study of these modifications generalizing the restricted example discussed by Bivona *et al.* [20].

In the past all theoretical investigations of LARR have been performed considering incident electrons that are described by a plane wave in the limit of infinite distance between the recombining electron and the parent nucleus. These plane-wave-like electrons only carry spin angular momentum. In contrast to that recently

it has been recently found by Bliokh et al. [26] that, free electrons may carry also a well defined amount of orbital angular momentum along their quantization axis. A few years ago these theoretical predictions have been verified experimentally and much effort has been spent to generate free electrons with high values of orbital angular momentum [27, 28] and to make them available for continuative experiments [29, 30]. The experimental availability of such *electron vortex beams* or *twisted* electrons triggered a bunch of theoretical studies characterizing their properties [31, 32]. Moreover possible applications in atomic physics have been investigated [33, 34]. Particularly RR with incident twisted electrons has been adressed lately [35]. At the same time the interaction of vortex electrons with laser fields has been explored [36]. Combining the findings of these works and our theory we present the first study of laser assisted processes involving twisted electrons using the example of LARR.

To achieve the aims set above we organize the present work as follows. The second chapter of this thesis is attributed to the description of electrons in external laser fields. There we put special emphasis on vortex solutions of the time dependent Schrödinger equation, i.e. we derive wave functions of laser driven twisted electrons. Moreover we recall the derivation of so called separable Coulomb-Volkov (SCV) wave functions which approximately describe electrons propagating in the superposition of an external electromagnetic and the Coulomb potential of an atomic nucleus. In Ch. 3 we will show how these wave functions can be used to express observable quantities using the S-matrix theory. Having derived explicit expressions for the (angle-differential) cross section of LARR and the polarization properties of the emitted recombination radiation in Ch. 4 we discuss numerical results in Ch. 5 considering plane-wave-like as well as twisted incoming electrons. We will conclude this work with a short summary of our findings and an outlook of possible topics to be addressed in the future.

2

THEORY OF ELECTRONS IN EXTERNAL LASER FIELDS

Before we set up a theory for LARR, we need to know how electrons can be described if they are exposed to an electromagnetic field. We go about such a description by applying the principal of minimal coupling to the interaction between the electron with momentum operator $\hat{\boldsymbol{p}}$ and the external laser field. This principal implies that, in Coulomb gauge, the electron-laser interaction can be incorporated into the Hamiltonian of the system by performing the following replacement:

$$\hat{\boldsymbol{p}} \mapsto \hat{\boldsymbol{p}} + \boldsymbol{A}(\boldsymbol{r}, t), \tag{2.1}$$

where $\boldsymbol{A}(\boldsymbol{r}, t)$ is the vector potential of the external laser field.

In this work we restrict ourselves to optical external lasers. Such lasers have a wavelength $\lambda_L = 380\,\mathrm{nm} \ldots 780\,\mathrm{nm}$ much larger than the typical atomic scale $a_0 = 0.05\,\mathrm{nm}$. Thus the so called *dipole approximation* is applicable. In this approximation the electric field $\boldsymbol{E}_L(t)$ of the laser is spatially homogeneous and, hence, only time dependent. For a linearly polarized laser with frequency ω_L we can write

$$\boldsymbol{E}_L(t) = \mathcal{E}_L \boldsymbol{\epsilon}_L \sin(\omega_L t), \tag{2.2}$$

where $\mathcal{E}_L$ is the electric field amplitude of the laser field and $\boldsymbol{\epsilon}_L$ its polarization. The corresponding vector potential that later enters the Hamiltonian via Eq. (2.1) is

$$\boldsymbol{A}_L(t) = \frac{\mathcal{E}_L}{\omega_L} \boldsymbol{\epsilon}_L \cos \omega_L t. \tag{2.3}$$

Instead of the electric field amplitude, the strength of a laser is commonly characterized by its intensity I_L that is related to $\mathcal{E}_L$ via (in SI units)

$$I_L = \frac{c\epsilon_0}{2} \mathcal{E}_L^2, \tag{2.4}$$

where c is the speed of light in vacuum and ϵ_0 the vacuum permittivity.

2.1 LASER DRIVEN ELECTRONS IN VACUUM

If an electron in vacuum, i.e. in absence of an atomic nucleus, is exposed to an external laser field we speak of a *free* and *laser driven* electron. We can obtain the Hamiltonian of such a free electron using Eq. (2.1):

$$\begin{aligned}\hat{H}_{free}(t) =& \frac{1}{2}\left(\hat{\boldsymbol{p}} + \boldsymbol{A}_L(t)\right)^2 \\ =& \frac{\hat{\boldsymbol{p}}^2}{2} + \boldsymbol{A}_L(t)\cdot\hat{\boldsymbol{p}} + \frac{1}{2}\boldsymbol{A}_L(t)^2.\end{aligned} \tag{2.5}$$

Here we made use of the fact that a $\boldsymbol{A}_L(t)$ yields the Coulomb gauge condition and therefore commutes with $\hat{\boldsymbol{p}}$. Below we will discuss two types of electrons that are described by this Hamiltonian.

2.1.1 *Volkov solution of the Schrödinger equation*

The Hamiltonian (2.5) describes an electron in vacuum with energy E_i and momentum $\boldsymbol{p}$ that interacts with a spatially homogeneous laser field with frequency ω_L and electric field amplitude $\mathcal{E}_L$. The wave function $\chi_{\boldsymbol{p}}^V(\boldsymbol{r},t)$ of this electron is a solution of the time dependent Schrödinger equation (TDSE) with Hamiltonian (2.5):

$$\mathrm{i}\partial_t\chi_{\boldsymbol{p}}^V(\boldsymbol{r},t) = \hat{H}_{free}\chi_{\boldsymbol{p}}^V(\boldsymbol{r},t). \tag{2.6}$$

To simplify this equation it is convenient to perform the gauge transformation

$$\widetilde{\chi}_{\boldsymbol{p}}^V(\boldsymbol{r},t) = \exp\left(\mathrm{i}\int_{-\infty}^{t}\mathrm{d}\tau\, A_L(\tau)^2\right)\chi_{\boldsymbol{p}}^V(\boldsymbol{r},t). \tag{2.7}$$

Equation (2.6) then becomes

$$\mathrm{i}\partial_t\widetilde{\chi}_{\boldsymbol{p}}^V(\boldsymbol{r},t) = \left(\frac{\hat{\boldsymbol{p}}^2}{2} + \boldsymbol{A}_L(t)\cdot\hat{\boldsymbol{p}}\right)\widetilde{\chi}_{\boldsymbol{p}}^V(\boldsymbol{r},t), \tag{2.8}$$

where the term proportional to $\boldsymbol{A}_L(t)^2$ dropped out due to the transformation. The exact solution $\widetilde{\chi}_{\boldsymbol{p}}^V(\boldsymbol{r},t)$ of Eq. (2.8) is the well known Volkov wave function that reads

$$\widetilde{\chi}_{\boldsymbol{p}}^V(\boldsymbol{r},t) = (2\pi)^{-3/2}\exp\left(\mathrm{i}\boldsymbol{p}\cdot\boldsymbol{r} - \mathrm{i}\boldsymbol{\alpha}_L(t)\cdot\boldsymbol{p} - \mathrm{i}E_i t\right), \tag{2.9}$$

where $\boldsymbol{\alpha}_L(t) = \mathcal{E}_L/\omega_L^2\sin(\omega_L t)\boldsymbol{\epsilon}_L$ is the amplitude of the quiver motion the electron performs in the laser field. Here it is noteworthy that the wave function (2.9) is a plane wave multiplied by a time dependent phase.

2.1.2 *Volkov-Bessel electrons*

Above we discussed solutions of the TDSE (2.6) for free electrons in an external laser field. We have shown that these solutions (2.9) are Volkov wave functions with a plane-wave-like spatial structure. Nowadays however there is rising interest in superpositions of plane-wave-like states to construct electron beams with novel properties. Cylindrically symmetric *electron vortex beams* are one example for this trend. In contrast to Volkov electrons they carry a well defined amount of orbital angular momentum l. Experimentally it is possible to produce such electron vortices with angular momenta up to $l = 100$ using holographic plates [29]. In theory electron vortex beams are constructed by superimposing plane-wave-like solutions with momentum $\boldsymbol{p}$ along a cone in momentum space. This cone has a certain radius $\varkappa$ and opening angle $\theta_p = \arcsin(\varkappa/p)$. Physically $\varkappa$ is the transverse momentum of the vortex electron we aim to construct. Following Refs. [35, 36] we describe the momentum cone by a weighting function

$$a_{l,\varkappa}(\boldsymbol{p}_\perp) = \delta(p_\perp - \varkappa)\frac{e^{\mathrm{i}l\varphi_p}}{2\pi \mathrm{i}^l \varkappa}, \tag{2.10}$$

where $\boldsymbol{p}_\perp$ is the component of the plane-wave-electron momentum $\boldsymbol{p}$ that is orthogonal to the z-axis of the reference frame. The direction of $\boldsymbol{p}_\perp$ is defined by the polar angle φ_p.

As mentioned above, the spatial structure of a Volkov electron (2.9) is plane-wave-like. Therefore we can superimpose Volkov wave functions (2.9) using the weighting function (2.10) to construct an electron vortex beam in an external laser field:

$$\begin{aligned}\widetilde{\chi}^{VB}_{\boldsymbol{p}}(\boldsymbol{r},t) &= \int_0^\infty \mathrm{d}p_\perp \int_0^{2\pi} \mathrm{d}\varphi_p \, p_\perp a_{l,\varkappa}(\boldsymbol{p}_\perp)\widetilde{\chi}^{V}_{\boldsymbol{p}}(\boldsymbol{r},t) \\ &= \int_0^\infty \mathrm{d}p_\perp \int_0^{2\pi} \mathrm{d}\varphi_p \, \exp\left(\mathrm{i}l\varphi_p + \mathrm{i}\boldsymbol{p}\cdot\boldsymbol{r} - \mathrm{i}\boldsymbol{\alpha}_L(t)\cdot\boldsymbol{p} - \mathrm{i}E_i t\right) \\ &\quad \times (2\pi)^{-3/2}\frac{\delta(p_\perp - \varkappa)}{2\pi\mathrm{i}^l\varkappa} p_\perp .\end{aligned} \tag{2.11}$$

Both integrals in this equation can be solved analytically. In order to perform the integration over the transverse component of the electron momentum we make use of the following relations:

$$\boldsymbol{p}\cdot\boldsymbol{r} = p_\perp r \sin\theta\cos(\varphi_p - \varphi) + p_z r\cos\theta, \tag{2.12a}$$

$$\boldsymbol{\alpha}_L(t)\cdot\boldsymbol{p} = p_\perp \alpha_L(t)\sin\theta_L\cos(\varphi_p - \varphi_L) + p_z\alpha_L(t)\cos\theta_L, \tag{2.12b}$$

where the angles θ_L and φ_L define the polarization direction of the external laser and $\alpha_L(t) = |\boldsymbol{\alpha}_L(t)|$. After inserting the relations (2.12) into Eq. (2.11) we can readily perform the integration over $p_\perp$ resolving the delta function in Eq. (2.11). The remaining integral over the polar angle φ_p reads

$$\begin{aligned}\widetilde{\chi}_{\boldsymbol{p}}^{VB}(\boldsymbol{r},t) =& \frac{\mathrm{i}^{-l}}{(2\pi)^{5/2}} \exp\left[\mathrm{i}p_z\left(r\cos\theta - \alpha_L(t)\cos\theta_L\right) - \mathrm{i}E_i t\right] \\ & \int_0^{2\pi} \mathrm{d}\varphi_p \, \exp\left[\mathrm{i}l\varphi_p + \mathrm{i}\varkappa r\sin\theta\cos(\varphi_p - \varphi)\right] \\ & \times \exp\left[-\mathrm{i}\alpha_L(t)\sin\theta_L\cos(\varphi_p - \varphi_L)\right].\end{aligned} \tag{2.13}$$

To solve this integral over φ_p, we use the Jacobi-Anger expansion

$$\mathrm{e}^{\mathrm{i}\varkappa r\sin\theta\cos(\varphi_p-\varphi)} = \sum_{n=-\infty}^{\infty} \mathrm{i}^n \mathrm{J}_n(\varkappa r\sin\theta)\,\mathrm{e}^{\mathrm{i}n(\varphi_p-\varphi)}, \tag{2.14a}$$

$$\mathrm{e}^{-\mathrm{i}\varkappa\alpha_L(t)\sin\theta_L\cos(\varphi_p-\varphi_L)} = \sum_{n'=-\infty}^{\infty} \mathrm{i}^{-n'} \mathrm{J}_{n'}\left(\varkappa\alpha_L(t)\sin\theta_L\right)\,\mathrm{e}^{\mathrm{i}n'(\varphi_p-\varphi_L)}, \tag{2.14b}$$

where $\mathrm{J}_n(x)$ is the Bessel function of the first kind. From the integration over φ_p we get another delta function that resolves the infinite summation over n'. Finally the wave function of the twisted electron is:

$$\begin{aligned}\widetilde{\chi}_{\boldsymbol{p}}^{VB}(\boldsymbol{r},t) =& \frac{(-1)^l}{(2\pi)^{3/2}} \exp\left[\mathrm{i}p_z\left(r\cos\theta - \alpha_L(t)\cos\theta_L\right) - \mathrm{i}E_i t\right] \\ & \times \sum_{n=-\infty}^{\infty} \mathrm{J}_{n+l}(\varkappa r\sin\theta)\mathrm{J}_n\left(\varkappa\alpha_L(t)\sin\theta_L\right)\exp[\mathrm{i}(l+n)\varphi + \mathrm{i}n\varphi_L].\end{aligned} \tag{2.15}$$

Because of their Bessel-like structure we will refer to the electrons described by the wave function above as *Volkov-Bessel* electrons.

To illustrate the properties of Volkov-Bessel electrons we show in Fig. 2.1 the probability density $|\widetilde{\chi}_{\boldsymbol{p}}^{VB}(\boldsymbol{r},t)|^2$ at three different times for two directions of the laser polarization. It can be seen in the figure that the center of the distribution propagates along the classical trajectory parallel to the polarization of the laser field. In the relativistic regime such Volkov-Bessel electrons have been discussed in detail in Ref. [36].

2.2 ATOMIC ELECTRONS IN A LASER FIELD

In the previous section we presented exact solutions of the TDSE for electrons in a spatially homogeneous laser field. We have shown that these solutions can be

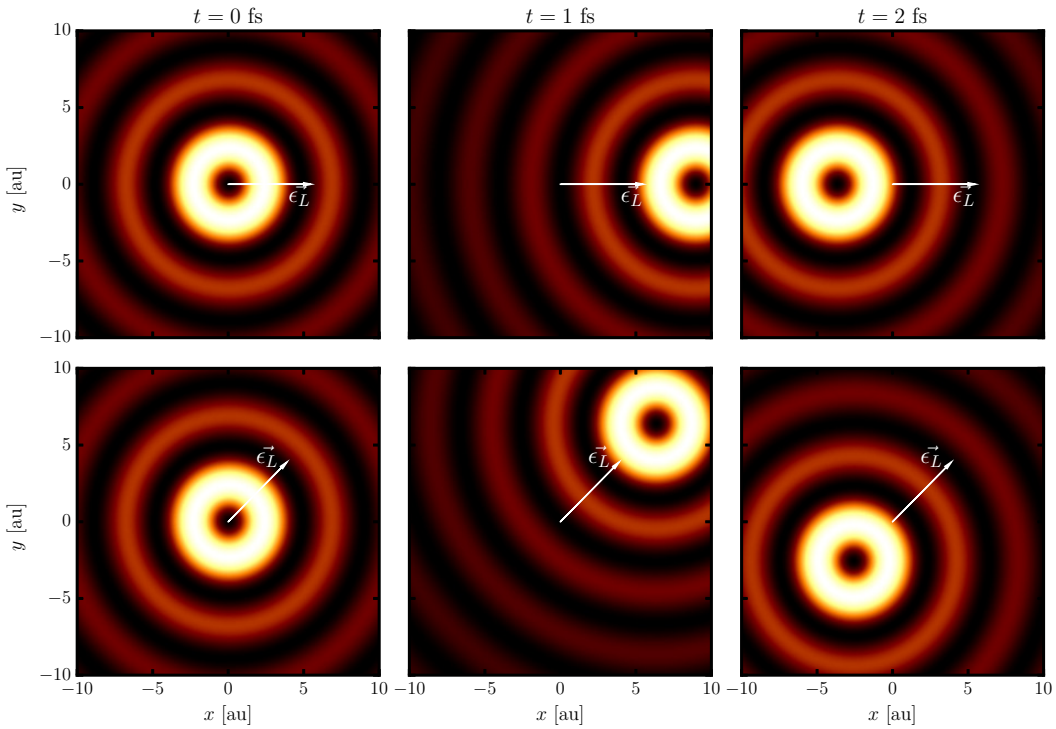

Figure 2.1: Electron density $|\widetilde{\chi}_{\boldsymbol{p}}^{VB}(\boldsymbol{r}, t)|^2$ of a 25 eV Volkov-Bessel electron with $\theta_p = 30°$ and orbital angular momentum $l = 1$ at $z = 0$ and three different times $t = 0$ fs (left column), $t = 1$ fs (center column), $t = 2$ fs (right column). Results are shown for two polarization directions of the laser $\varphi_L = 0°$ (upper row) and $\varphi_L = 45°$ (lower row) perpendicular to the beam axis ($\theta_p = 90°$). The laser parameters are $I_L = 10^{13}\,\mathrm{W/cm^2}$ and $\omega_L = 1.17$ eV.

constructed in such a way that they are eigenfunctions of the orbital angular momentum operator with a Besse-like electron density distribution. The investigation of laser assisted atomic processes however demands the description of electrons propagating in the superposition of two fields: The fields of the atomic nucleus and the external laser. The corresponding Hamiltonian now includes the Coulomb potential of a nucleus with charge Z. It reads:

$$\hat{H}(t) = \frac{\hat{\boldsymbol{p}}^2}{2} - \frac{Z}{r} + \boldsymbol{A}_L(t) \cdot \hat{\boldsymbol{p}} + \frac{1}{2}\boldsymbol{A}_L(t)^2. \tag{2.16}$$

For our later discussion it is convenient to split this Hamiltonian into two parts

$$\hat{H}_{at} = \frac{\hat{\boldsymbol{p}}^2}{2} - \frac{Z}{r}, \tag{2.17a}$$

$$\hat{H}_{int}(t) = \boldsymbol{A}_L(t) \cdot \hat{\boldsymbol{p}} + \frac{1}{2}\boldsymbol{A}_L(t)^2, \tag{2.17b}$$

where $\hat{H}_{at}$ is the well known time independent atomic Hamiltonian and $\hat{H}_{int}(t)$ characterizes the interaction between the electron and the external laser field. An exact solution for the TDSE with Hamiltonian (2.16) is not known, therefore it is necessary to apply proper approximations. The nature of these approximations depends on the considered electron state. For a continuum electron the strength of the laser field is much larger than the atomic potential, while the latter exceeds the laser field if the electron is in a lower bound state. Therefore we will below derive two types of approximate solutions for continuum and bound electrons, respectively.

2.2.1 *Separable Coulomb Volkov continuum*

We have already sketched the derivation of the Volkov wave function (2.9) of a free electron in an external laser field as an exact solution of the TDSE with Hamiltonian $\hat{H}_{free}(t)$ (2.5). If the electron is not free but in a continuum state of a hydrogen like ion we have to account for the additional Coulomb potential of the nucleus, however it is small compared to the driving laser field.

A well established approach to describe continuum electrons in a laser field has been developed by Jain and Tzoar [37]. They construct so called *separable Coulomb-Volkov* (SCV) continuum states based on the assumption that the electron is mainly influenced by the external laser. Therefore the starting point for the derivation of a SCV state is the Volkov wave function $\widetilde{\chi}_{\boldsymbol{p}}^{V}(\boldsymbol{r}, t)$ that has a plane-wave-like spatial structure given by $(2\pi)^{-3/2}\exp(\mathrm{i}\boldsymbol{k}\cdot\boldsymbol{r})$. Following Ref. [37] we embed the influence of the nucleus on the electron by replacing this exponential plane wave term with the continuum wave function of a hydrogen like ion (see e.g. [38])

$$\phi_{\boldsymbol{p}}(\boldsymbol{r}) = (2\pi)^{-\frac{3}{2}}\, \mathrm{e}^{\frac{\pi Z}{2p} + \mathrm{i}\boldsymbol{p}\cdot\boldsymbol{r}}\Gamma(1 - \mathrm{i}Z/p)\,{}_1\mathrm{F}_1[\mathrm{i}Z/p, 1, \mathrm{i}(pr - \boldsymbol{p}\cdot\boldsymbol{r})], \tag{2.18}$$

where $\Gamma(x)$ is the Euler gamma function and ${}_1F_1(a, b, z)$ the confluent hypergeometric function. After replacing the plane wave in Eq. (2.9) by Eq. (2.18) we obtain

the approximate wave function for an electron in the combined field of a nucleus and an external laser:

$$\begin{aligned}\widetilde{\chi}_{\boldsymbol{p}}^{SCV}(\boldsymbol{r},t) =&(2\pi)^{-\frac{3}{2}}\Gamma(1-\mathrm{i}Z/p)_1\mathrm{F}_1[\mathrm{i}Z/p,1,\mathrm{i}(pr-\boldsymbol{p}\cdot\boldsymbol{r})]\\ &\times\exp\left(\mathrm{i}\boldsymbol{p}\cdot\boldsymbol{r}-\mathrm{i}\boldsymbol{\alpha}_L(t)\cdot\boldsymbol{p}-\mathrm{i}E_it+\frac{\pi Z}{2p}\right).\end{aligned} \tag{2.19}$$

We see that $\widetilde{\chi}_{\boldsymbol{p}}^{SCV}(\boldsymbol{r},t)$ still seperates into a phase-like time evolution and a spatial structure. It is important to notice that this wave function is neither an eigenfunction of $\hat{H}(t)$ (2.16) nor of $\hat{H}_{at}$ (2.17a), although the parts we used for its construction are. Regardless of this restriction Eq. (2.19) behaves properly in the high energy ($p\to\infty$) and vanishing field ($E_L\to 0$) limit. In these limits we recover the Volkov solution (2.9) for a free electron in a laser field or the continuum wave function of a hydrogen like ion (2.18), respectively.

After we made plausible that the wave function $\widetilde{\chi}_{\boldsymbol{p}}^{SCV}(\boldsymbol{r},t)$ (2.19) is an approximate description of a laser driven electron in a continuum state of a hydrogen like ion we need to discuss the validity of our idea. We will only sketch the arguments here and refer the reader to the literature for a more detailed discussion [37, 39]. In line with our assumptions made above to arrive at Eq. (2.19) the SCV approach is valid as long as the momentum transferred to the electron by the external laser field is much larger than the momentum of the free electron motion p. This momentum transfer is quantified by the prefactor $\boldsymbol{A}_L(t)$ in Eq. (2.16). Therefore the validity condition is:

$$|\boldsymbol{A}_L(t)|\ll p \tag{2.20}$$

or equivalently

$$\frac{\mathcal{E}_L}{\omega_L p}\ll 1. \tag{2.21}$$

To illustrate the parameter range in which the SCV wave function (2.19) properly describes a continuum electron in an external field we show in Fig. 2.2 the validity condition (2.21) for two thresholds $\mathcal{E}_L/(\omega_L p)<0.5$ (dashed lines) and $\mathcal{E}_L/(\omega_L p)<0.2$ (solid lines). The laser frequencies have been chosen to be $\omega_L=1.17\,\mathrm{eV}$ (black lines), the main line of a Nd:YAG laser that is often frequency doubled to $\omega_L=2.34\,\mathrm{eV}$ (blue lines). So the approximation (2.19) is valid as long as the considered parameters are *below* the corresponding lines plotted in Fig. 2.2. We see that up to laser intensities of $I_L=10^{13}\,\mathrm{W/cm^2}$ SCV wave functions deliver a reasonable description of laser driven continuum electrons with typical energies $E_i>10\,\mathrm{eV}$.

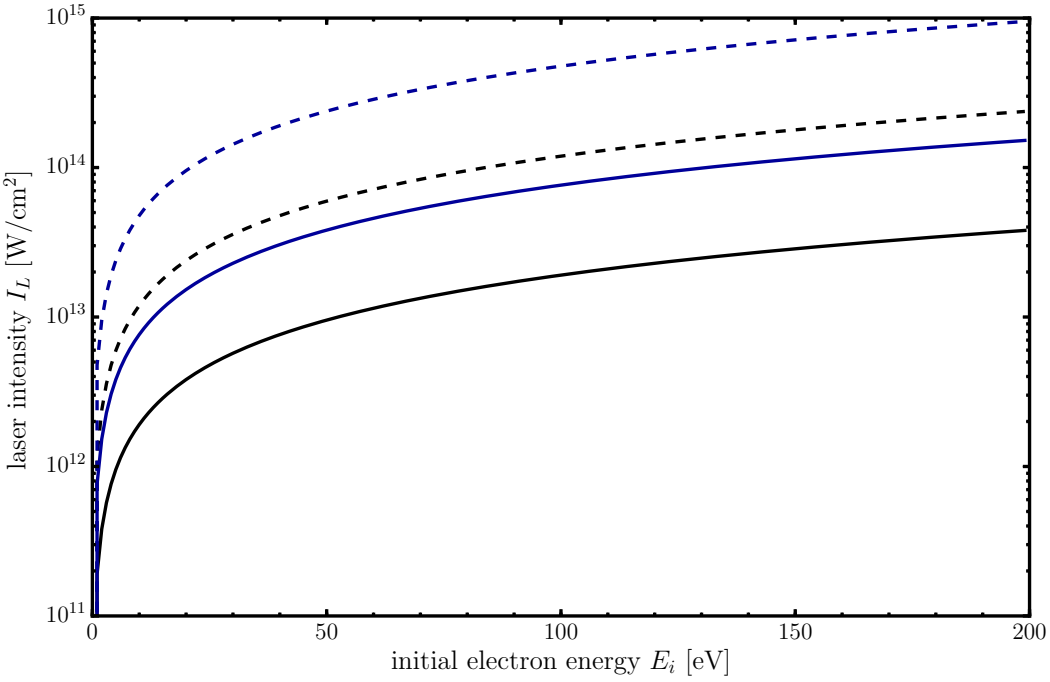

Figure 2.2: Validity condition (2.21) for the SCV continuum wave function for two different laser frequencies $\omega_L = 1.17\,\text{eV}$ (black lines) and $\omega_L = 2.34\,\text{eV}$ (blue lines). The solid and dashed lines refer to two different validity thresholds $\mathcal{E}_L/(\omega_L p) < 0.5$ (dashed lines) and $\mathcal{E}_L/(\omega_L p) < 0.2$ (solid lines). The theory is valid as long as the chosen parameters are below the shown lines.

2.2.2 *Perturbatively dressed bound states*

Up to now we obtained an approximate wave function for a continuum electron that is driven by an external laser field. Our derivations were based on the assumption that the Coulomb potential of the nucleus is much smaller than the vector potential $\boldsymbol{A}_L(t)$ of the laser. If the electron is not in the continuum but bound to the nucleus the situation is vice versa; the atomic potential exceeds $\boldsymbol{A}_L(t)$. Therefore we can treat the laser interaction given by $\hat{H}_{int}(t)$ within first order time dependent perturbation theory.

It is essential for our later purposes that all wave functions are obtained in the same gauge. Therefore we first need to perform the same gauge transformation as

we did to obtain Eq. (2.8). So the *laser dressed* wave function $\widetilde{\psi}_{nlm}(\boldsymbol{r},t)$ of a bound state electron in an external field is a solution of the following TDSE:

$$\mathrm{i}\partial_t\widetilde{\psi}_{nlm}(\boldsymbol{r},t) = \left(\frac{\hat{\boldsymbol{p}}^2}{2} - \frac{Z}{r} + \boldsymbol{A}_L(t)\cdot\hat{\boldsymbol{p}}\right)\widetilde{\psi}_{nlm}(\boldsymbol{r},t) \tag{2.22}$$

where nlm are the quantum numbers of the unperturbed hydrogenic state. As it is small we can now treat the term $\boldsymbol{A}_L(t)\cdot\hat{\boldsymbol{p}}$ perturbatively. Under the assumption that the laser is not in resonance with any atomic transition we follow Ref. [40] and obtain the perturbed bound state wave function:

$$\begin{aligned}\widetilde{\psi}_{nlm}(\boldsymbol{r},t) = \mathrm{e}^{-\mathrm{i}E_n t}\Bigg[\phi_{nlm}(\boldsymbol{r}) - \frac{\mathcal{E}_L}{2\omega_L}\sum_{n'l'm'}\left(\frac{\mathrm{e}^{\mathrm{i}\omega_L t}}{\omega_{n'n}+\omega_L} + \frac{\mathrm{e}^{-\mathrm{i}\omega_L t}}{\omega_{n'n}-\omega_L}\right)\\ \times\left\langle n'l'm'\,\middle|\,\boldsymbol{\epsilon}_L\cdot\hat{\boldsymbol{p}}\,\middle|\,nlm\right\rangle\phi_{n'l'm'}(\boldsymbol{r})\Bigg],\end{aligned} \tag{2.23}$$

where $\phi_{nlm}(\boldsymbol{r})$ are the unperturbed eigenfunctions of $\hat{H}_{at}$ (2.17a) in coordinate space and $|nlm\rangle$ the corresponding state vectors. Moreover we defined $\omega_{n'n} = E_{n'} - E_n$ where E_n is the energy of the unperturbed state with principal quantum number n. However, generally extended over the complete set of eigenfunctions of $\hat{H}_{at}$ we restricted the summation in the second term of Eq. (2.23) to the bound states of a hydrogen like ion.

We can further simplify Eq. (2.23) by making use of the Heisenberg equation of motion with respect to $\hat{H}_{at}$ (2.17a) to rewrite the matrix elements in the following way [40, 41]:

$$\left\langle n'l'm\,\middle|\,\boldsymbol{\epsilon}_L\cdot\hat{\boldsymbol{p}}\,\middle|\,nlm\right\rangle = \mathrm{i}\omega_{n'n}\left\langle n'l'm'\,\middle|\,\boldsymbol{\epsilon}_L\cdot\boldsymbol{r}\,\middle|\,nlm\right\rangle. \tag{2.24}$$

Eq. (2.23) then becomes:

$$\begin{aligned}\widetilde{\psi}_{nlm}(\boldsymbol{r},t) = \mathrm{e}^{-\mathrm{i}E_n t}\Bigg[\phi_{nlm}(\boldsymbol{r}) - \mathrm{i}\frac{\mathcal{E}_L}{2\omega_L}\sum_{n',l',m'}\left(\frac{\mathrm{e}^{\mathrm{i}\omega_L t}}{1+\frac{\omega_L}{\omega_{n'n}}} + \frac{\mathrm{e}^{-\mathrm{i}\omega_L t}}{1-\frac{\omega_L}{\omega_{n'n}}}\right)\\ \times\left\langle n'l'm'\,\middle|\,\boldsymbol{\epsilon}_L\cdot\boldsymbol{r}\,\middle|\,nlm\right\rangle\phi_{n'l'm'}(\boldsymbol{r})\Bigg].\end{aligned} \tag{2.25}$$

Within the limits of perturbation theory, this wave function is valid for any laser frequency ω_L, if not they are in resonance with an atomic transition. Yet, in the beginning of this chapter, we have restricted ω_L to the visible regime, which allows us to derive a very simple expression for the laser dressed wave function of the 1s hydrogen ground state. In this case we have $n = 1$ and the condition $\omega_L \ll$

$10.2\,\mathrm{eV} \leq \omega_{n'1}$ is satisfied, thus we can identify $1 + \omega_L/\omega_{n'1} \approx 1$. Applying this so called *soft photon approximation* we obtain:

$$\widetilde{\psi}_{1s}(\boldsymbol{r},t) = \mathrm{e}^{-\mathrm{i}E_1 t}\left(\phi_{100}(\boldsymbol{r}) - \mathrm{i}\frac{\mathcal{E}_L}{\omega_L}\cos(\omega_L t)\sum_{n'l'm'}\left\langle n'l'm' \,\middle|\, \boldsymbol{\epsilon}_L\cdot\boldsymbol{r} \,\middle|\, 100\right\rangle \phi_{n'l'm'}(\boldsymbol{r})\right). \tag{2.26}$$

Here the summation over the bound states in the second term can be performed explicitly using:

$$\begin{aligned}\sum_{n'l'm'}\left\langle n'l'm' \,\middle|\, \boldsymbol{\epsilon}_L\cdot\boldsymbol{r} \,\middle|\, 100\right\rangle \phi_{n'l'm'}(\boldsymbol{r}) &= \sum_{n'l'm'}\left\langle \boldsymbol{r} \,\middle|\, n'l'm'\right\rangle \left\langle n'l'm' \,\middle|\, \boldsymbol{\epsilon}_L\cdot\boldsymbol{r} \,\middle|\, 100\right\rangle \\ &= \left\langle \boldsymbol{r} \,\middle|\, \boldsymbol{\epsilon}_L\cdot\boldsymbol{r} \,\middle|\, 100\right\rangle \\ &= \boldsymbol{\epsilon}_L\cdot\boldsymbol{r}\,\phi_{100}(\boldsymbol{r}).\end{aligned} \tag{2.27}$$

Finally we get the following expression for the laser dressed ground state of a hydrogen like ion in soft photon approximation:

$$\widetilde{\psi}_{1s}(\boldsymbol{r},t) = \mathrm{e}^{-\mathrm{i}E_1 t}\phi_{100}(\boldsymbol{r})\left(1 - \mathrm{i}\frac{\mathcal{E}_L}{\omega_L}\boldsymbol{\epsilon}_L\cdot\boldsymbol{r}\cos(\omega_L t)\right). \tag{2.28}$$

The first term in parenthesis is the unperturbed hydrogen ground state wave function, while the second term, *dressing term*, arises due to the laser dressing of the ground state. Our perturbative approach is valid as long as this second term is much smaller than one. Therefore the validity condition reads:

$$\frac{\mathcal{E}_L}{\omega_L} \ll 1 \tag{2.29}$$

where we assumed $|\boldsymbol{r}| = a_0$ to be the typical length scale. As an example for $\omega_L = 1.17\,\mathrm{eV}$ and $I_L = 10^{13}\,\mathrm{W/cm^2}$ we get the ratio $\mathcal{E}_L/\omega_L \approx 0.4$ and for the same intensity but $\omega_L = 2.34\,\mathrm{eV}$ it is $\mathcal{E}_L/\omega_L \approx 0.2$.

In the next chapter we will show how wave functions of the kind we derived up to now can be used to describe atomic processes. Afterwards we will proceed with explicit calculations for the laser assisted recombination of electrons into the ground state of hydrogen like ions.

3

S-MATRIX THEORY FOR ATOMIC PROCESSES

Usually atomic processes are understood as the transition from an ingoing state $|\psi_i\rangle$ that interacts with a potential $\hat{V}(t)$ to an outgoing state $\langle\psi_f|$. It was Heisenberg's idea to use the so called *scattering matrix* or *S-matrix* to describe observable quantities related to such processes. In this chapter we will outline how these matrices and the corresponding observables are constructed.

Imagine a given system whose Hamiltonian splits into a time independent part $\hat{H}_0$ and a time dependent interaction potential $\hat{V}(t)$ such that

$$\hat{H}(t) = \hat{H}_0 + \hat{V}(t). \tag{3.1}$$

To derive the S-matrix for the transition from $|\psi_i\rangle$ to $\langle\psi_f|$ via the interaction with $\hat{V}(t)$ it is convenient to express the interaction operator in the Dirac picture:

$$\hat{V}_D(t) = \mathrm{e}^{\mathrm{i}\hat{H}_0 t}\hat{V}(t)\,\mathrm{e}^{-\mathrm{i}\hat{H}_0 t}. \tag{3.2}$$

The S-matrix is then defined as

$$S_{fi} = \left\langle \psi_f \,\middle|\, \hat{T}\exp\left(-\mathrm{i}\int_{-\infty}^{\infty}\mathrm{d}t\,\hat{V}_D(t)\right)\,\middle|\,\psi_i\right\rangle \tag{3.3}$$

where $\hat{T}$ is the Dyson time ordering operator. It is easier to interprete this general definition of a S-matrix if we expand the exponential term in Eq. (3.3) in a Dyson series:

$$\begin{aligned} S_{fi} = \langle\psi_f\,|\,\hat{\mathbb{1}}\,|\,\psi_i\rangle - \mathrm{i}\left\langle\psi_f\,\middle|\,\int_{-\infty}^{\infty}\mathrm{d}t_1\,\hat{V}_D(t_1)\,\middle|\,\psi_i\right\rangle \\ - \left\langle\psi_f\,\middle|\,\int_{-\infty}^{\infty}\mathrm{d}t_1\int_{-\infty}^{t_1}\mathrm{d}t_2\,\hat{V}_D(t_1)\hat{V}_D(t_2)\,\middle|\,\psi_i\right\rangle + \dots. \end{aligned} \tag{3.4}$$

The addends in this expansion can be understood as different orders of perturbations. The first term in Eq. (3.4) is the no-scattering term, that describes the transition from the initial to the final state without any interaction. This term vanishes always unless $|\psi_i\rangle = |\psi_f\rangle$. For the special case of $\hat{V}(t)$ being an electromagnetic vector potential we will develop a more figurative interpretation of the different perturbative orders below.

3.1 S-MATRIX FORMALISM OF ONE PHOTON PROCESSES

Up to now we gave general expressions and interpretations of the S-matrix for an arbitrary interaction operator. Moreover we have shown that the S-matrix can be decomposed into a Dyson series. In this section we will discuss the physical meaning of this expansion. If the transition between the initial and the final state $|\psi_i\rangle$ and $\langle\psi_f|$ involves the emission or absorption of one or more photons with frequency ω_k the interaction operator is given by an electromagnetic vector potential that reads generally

$$\hat{V}_{ph}(\boldsymbol{r},t) = \hat{A}(\boldsymbol{r})\,\mathrm{e}^{-\mathrm{i}\omega_k t} + \hat{A}^\dagger(\boldsymbol{r})\,\mathrm{e}^{\mathrm{i}\omega_k t}, \tag{3.5}$$

where the first term describes the absorption and the second the emission of a photon. In our considerations we assume the emitted or absorbed photon to be a plane wave. In this case we have

$$\hat{A}(\boldsymbol{r}) = -\mathrm{i}\,\mathrm{e}^{\mathrm{i}\boldsymbol{k}\cdot\boldsymbol{r}}\boldsymbol{\epsilon}_k \cdot \nabla, \tag{3.6}$$

where $\boldsymbol{\epsilon}_k$ is the polarization and $\boldsymbol{k}$ the momentum of the photon.

Knowing now that (3.5) describes the emission or absorption of *one* photon we can interprete the different orders of $\hat{V}(t)$ in Eq. (3.4) as different numbers of photons that are exchanged during the interaction with $\hat{V}(t)$. The no-scattering term for example reflects the case where no photon participates in the process. The second term describes the emission or absorption of one photon as it is the case in the ordinary photoeffect or radiative recombination. Higher order terms may represent multi photon processes, for instance above threshold ionization. This work is attributed to laser assisted radiative recombination where only one photon is emitted during the process. Therefore we later need to calculate the first order S-matrix that is

$$S_{fi} = -\mathrm{i}\int_{-\infty}^{\infty}\mathrm{d}t\ \left\langle \psi_f(\boldsymbol{r},t)\,\middle|\,\hat{V}_{ph}(\boldsymbol{r},t)\,\middle|\,\psi_i(\boldsymbol{r},t)\right\rangle, \tag{3.7}$$

where we switched to the Schrödinger picture again by acting with the time evolution operators $\exp(\pm\mathrm{i}\hat{H}_0 t)$ on the state vectors.

3.2 DIFFERENTIAL AND TOTAL CROSS SECTION

As we already indicated, one of the advantages of using S-matrices for the description of atomic processes is their direct relation to the total and differential cross

section of the process. In order to derive expressions for this relation we first need to define the so called *matrix element* $\mathcal{M}_{fi}$:

$$S_{fi} = 2\pi \mathrm{i}\delta \left(\sum_i^{N_i} E_{p_i} - \sum_i^{N_f} E'_{p_i} \right) \mathcal{M}_{fi}, \tag{3.8}$$

where N_i and N_f are the numbers of in- and outgoing particles. Momentum and energy of the i-th particle are represented by $\boldsymbol{p}_i$ and $E_{p_i} = p_i^2/2$, respectively. With regard to LARR we can restrict ourselves to one ingoing and two outgoing particles, thus Eq. (3.8) reduces to

$$S_{fi} = 2\pi \mathrm{i}\delta \left(E_a - E'_a - E_b \right) \mathcal{M}_{fi}. \tag{3.9}$$

With this definition in hand we can use Fermi's golden rule to write down the corresponding differential cross section $\mathrm{d}\sigma$ given by

$$\mathrm{d}\sigma = \frac{2\pi}{2E_a p_a} \delta \left(E_a - E'_a - E_b \right) \left| \mathcal{M}_{fi} \right|^2 \frac{\mathrm{d}^3 \boldsymbol{p}'_a}{2E'_a (2\pi)^3} \frac{\mathrm{d}^3 \boldsymbol{p}_b}{2E_b (2\pi)^3}. \tag{3.10}$$

Based on this equation, the total cross section σ can be obtained by integrating over all degrees of freedom of the outgoing particles:

$$\sigma = \int_{p'_a} \frac{\mathrm{d}^3 \boldsymbol{p}'_a}{2E'_a (2\pi)^3} \int_{p_b} \frac{\mathrm{d}^3 \boldsymbol{p}_b}{2E_b (2\pi)^3} \frac{2\pi}{2E_a p_a} \delta \left(E_a - E'_a - E_b \right) \left| \mathcal{M}_{fi} \right|^2, \tag{3.11}$$

where one degree of freedom is already fixed by energy conservation, expressed by the delta function $\delta \left(E_a - E'_a - E_b \right)$.

4 THEORY OF LASER ASSISTED RADIATIVE RECOMBINATION

In the previous chapter we have shown how atomic processes can be described using S-matrices. Moreover we have related these S-matrices to the corresponding cross sections via Fermi's golden rule. Having LARR in mind we already refined the general expressions presented above for the description of one photon processes with one ingoing and two outgoing particles. In this chapter we will use these specialized equations (3.9) and (3.10) to derive analytical expressions for the differential and total cross section of LARR. We will perform these derivations for two different kinds of incoming electrons (i) Coulomb-Volkov like solutions (2.19) and (ii) Volkov-Bessel electrons (2.15).

4.1 LASER FREE RADIATIVE RECOMBINATION

Before we start our discussion of LARR we would like to recall the characteristics of laser free radiative recombination (RR). We will spend some effort on the details here because we will later refer to the results obtained in this section.

4.1.1 *Geometry*

In this paragraph we will briefly explain the geometry we use as a basis for our description of RR. Fig. 4.1 displays this geometry in the rest frame of the atom with which the electron recombines. We choose the incident electron momentum $\boldsymbol{p}$ to lie along the z-axis which is also the quantization axis. The momentum of the emitted recombination photon $\boldsymbol{k}$ together with $\boldsymbol{p}$ defines the xz-plane. We will call the angle θ_k between those two vectors the *photon emission angle* while the *polarization angle* χ defines the direction of the photon polarization $\boldsymbol{\epsilon}_k$.

4.1.2 *Differential and total cross section*

To obtain an expression for the S-matrix and thus the differential and total cross section of RR we need to specify the in- and and outgoing state. In our study we

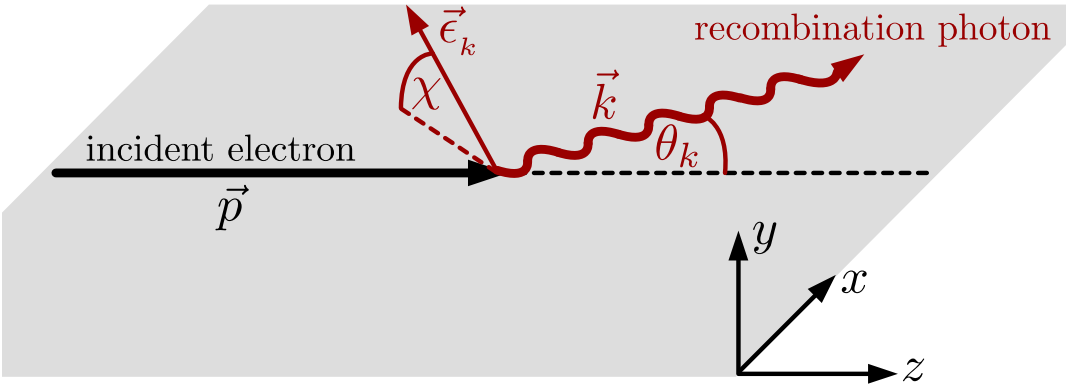

Figure 4.1: Geometry of radiative recombination. The z-axis is chosen along the incident electron momentum $\boldsymbol{p}$. The xz-plane is defined by $\boldsymbol{p}$ and the momentum vector of the outgoing photon $\boldsymbol{k}$. The direction of $\boldsymbol{k}$ is given by its polar angle θ_k. The polarization direction of the emitted photon is given by $\boldsymbol{\epsilon}_k$ and characterized by the angle χ

will restrict ourselves to the case where a continuum electron (2.18) is captured into the $1s$ ground state of a hydrogen like ion given by:

$$\langle \boldsymbol{r}|100\rangle = \phi_{100}(r) = \sqrt{\frac{Z^3}{\pi}}\,\mathrm{e}^{-Zr}. \tag{4.1}$$

Recalling that $\hat{V}(t) = \exp[\mathrm{i}(\omega_k t - \boldsymbol{k}\cdot\boldsymbol{r})t]$ describes the emission of one photon with momentum $\boldsymbol{k}$ and frequency ω_k we can now use the definition (3.7) and write down the S-matrix for the radiative recombination of an electron with momentum $\boldsymbol{p}$ into the ground state of a hydrogen like ion:

$$\mathcal{S} = -\mathrm{i}\int_{-\infty}^{\infty}\mathrm{d}t\,\left\langle 100\,\middle|\,\mathrm{e}^{\mathrm{i}\hat{H}_{at}t}\,\mathrm{e}^{\mathrm{i}(\omega_k t-\boldsymbol{k}\cdot\boldsymbol{r})}(\boldsymbol{\epsilon}_k\cdot\nabla)\,\mathrm{e}^{-\mathrm{i}\hat{H}_{at}t}\,\middle|\,\phi_{\boldsymbol{p}}\right\rangle. \tag{4.2}$$

We can further simplify this equation by applying the *dipole approximation* for the emitted photon. In this approximation, that is justified for all examples shown in this work, the inequality $\boldsymbol{k}\cdot\boldsymbol{r} \ll 1$ holds. Therefore we may write:

$$\begin{aligned}\mathcal{S} &= -\,\mathrm{i}\int_{-\infty}^{\infty}\mathrm{d}t\,\left\langle 100\,\middle|\,\mathrm{e}^{\mathrm{i}(E_1+\omega_k-E_i)t}(\boldsymbol{\epsilon}_k\cdot\nabla)\,\middle|\,\phi_{\boldsymbol{p}}\right\rangle \\ &= -\,2\pi\mathrm{i}\delta(E_i-E_1-\omega_k)\int_{\mathbb{R}^3}\mathrm{d}^3\boldsymbol{r}\,\phi_{100}(r)(\boldsymbol{\epsilon}_k\cdot\nabla)\phi_{\boldsymbol{p}}(\boldsymbol{r}),\end{aligned} \tag{4.3}$$

where we made use of the fact the $|100\rangle$ as well as $|\phi_{\boldsymbol{p}}\rangle$ is an eigenfunction of the time evolution operator $\exp(\mathrm{i}\hat{H}_{at}t)$.

To derive an expression for the differential cross section of RR we need to find the matrix element $\mathcal{M}_{RR}(\boldsymbol{p}, Z)$ of the process. We can read it directly off the S-matrix shown in Eq. (4.3) above using Eq. (3.9) and find:

$$\mathcal{M}_{RR}(\boldsymbol{p}, Z) = -\int_{\mathbb{R}^3} \mathrm{d}^3\boldsymbol{r}\, \phi_{100}(r)(\boldsymbol{\epsilon}_k \cdot \nabla)\phi_{\boldsymbol{p}}(\boldsymbol{r}). \tag{4.4}$$

Integrating this equation by parts we obtain:

$$\begin{aligned}\mathcal{M}_{RR}(\boldsymbol{p}, Z) &= -\left.\phi_{\boldsymbol{p}}(\boldsymbol{r})\phi_{100}(r)\right|_{\partial\mathbb{R}^3} + \int_{\mathbb{R}^3} \mathrm{d}^3\boldsymbol{r}\, \phi_{\boldsymbol{p}}(\boldsymbol{r})(\boldsymbol{\epsilon}_k \cdot \nabla)\phi_{100}(r) \\ &= \int_{\mathbb{R}^3} \mathrm{d}^3\boldsymbol{r}\, \phi_{\boldsymbol{p}}(\boldsymbol{r})(\boldsymbol{\epsilon}_k \cdot \nabla)\phi_{100}(r),\end{aligned} \tag{4.5}$$

where the arising surface term has vanished in the second line since we require physical wave functions to be zero at infinity. We can now plug the explicit form of the wave functions $\phi_{100}(r)$ (4.1) and $\phi_{\boldsymbol{p}}(\boldsymbol{r})$ (2.18) into Eq. (4.5) and find

$$\mathcal{M}_{RR}(\boldsymbol{p}, Z) = 2^6\pi^3 B(\boldsymbol{\epsilon}_k \cdot \nabla_k)\mathcal{I}(\boldsymbol{p}, Z, \boldsymbol{k})\big|_{\boldsymbol{k}=0} \tag{4.6}$$

where ∇_k is the gradient with respect to the components of $\boldsymbol{k}$ and where we defined $B = -2\pi\mathrm{i}\sqrt{2Z^5}\exp(\pi Z/2p)\Gamma(1 - \mathrm{i}Z/p)$. The function $\mathcal{I}(\boldsymbol{p}, Z, \boldsymbol{k})$ is the well known atomic integral

$$\begin{aligned}\mathcal{I}(\boldsymbol{p}, Z, \boldsymbol{k}) =& \int_{\mathbb{R}^3} \frac{\mathrm{d}^3\boldsymbol{r}}{r}\, \mathrm{e}^{\mathrm{i}(p-\boldsymbol{k})\cdot\boldsymbol{r}}\, {}_1\mathrm{F}_1[\mathrm{i}Z/p, 1, \mathrm{i}(pr - \boldsymbol{p}\cdot\boldsymbol{r})] \\ =& 4\pi \frac{\left[k^2 + (Z - \mathrm{i}p)^2\right]^{-\mathrm{i}\frac{Z}{p}}}{\left[(\boldsymbol{p} - \boldsymbol{k})^2 + Z^2\right]^{1-\mathrm{i}\frac{Z}{p}}}\end{aligned} \tag{4.7}$$

that can be found e.g. in Refs. [42, 43]. After some algebra we obtain an explicit expression for the matrix element

$$\mathcal{M}_{RR}(\boldsymbol{p}, Z) = B(\boldsymbol{\epsilon}_k \cdot \boldsymbol{e}_p)\frac{p - \mathrm{i}Z}{(p^2 + Z^2)^2}\, \mathrm{e}^{-2\frac{Z}{p}\mathrm{arccot}\left(\frac{Z}{p}\right)}. \tag{4.8}$$

Inserting this equation into the general definition of the cross section of a one photon process (3.10) we obtain the well known Stobbe formula [44] for the cross section of RR:

$$\frac{\mathrm{d}\sigma^{1s}}{\mathrm{d}\Omega_k} = \frac{2^5\pi}{c^3}\left(\frac{Z^3}{p(Z^2 + p^2)}\right)^2 \frac{\mathrm{e}^{-4\frac{Z}{p}\mathrm{arccot}\left(\frac{Z}{p}\right)}}{1 - \mathrm{e}^{-2\pi\frac{Z}{p}}}\left|\boldsymbol{\epsilon}_k \cdot \boldsymbol{e}_p\right|^2, \tag{4.9}$$

where $\boldsymbol{e}_p = (0, 0, 1)$ is the unit vector pointing along the initial electron momentum.

Eq. (4.9) represents the angle-differential cross section of RR for a certain polarization $\boldsymbol{\epsilon}_k$ of the emitted recombination photon. If, in contrast, we want to describe RR assuming that the polarization of the emitted photon is not observed we need to polarization average the cross section $\mathrm{d}\sigma^{1s}/\mathrm{d}\Omega_k$ (4.9). This can be done by making use of the relation [42]

$$\sum_{\boldsymbol{\epsilon}_k} \left|\boldsymbol{\epsilon}_k \cdot \boldsymbol{e}_p\right|^2 = 1 - \left|\boldsymbol{e}_k \cdot \boldsymbol{e}_p\right|^2 = \sin^2\theta_k \tag{4.10}$$

for the sum over all possible $\boldsymbol{\epsilon}_k$. The polarization averaged angle-differential cross section, which we will call *angular distribution*, can be then written as:

$$\frac{\overline{\mathrm{d}\sigma^{1s}}}{\mathrm{d}\Omega_k} = \frac{2^5\pi}{c^3}\left(\frac{Z^3}{p(Z^2+p^2)}\right)^2 \frac{\mathrm{e}^{-4\frac{Z}{p}\operatorname{arccot}\left(\frac{Z}{p}\right)}}{1-\mathrm{e}^{-2\pi\frac{Z}{p}}}\sin^2\theta_k. \tag{4.11}$$

We immediately see from this equation that the angular distribution has a $\sin^2\theta_k$ shape that forbids the emission of the recombination photon in the forward ($\theta_k = 0°$) or backward ($\theta_k = 180°$) direction.

Up to now we have derived expressions for the angle-differential cross section where we either averaged over all possible polarizations of the recombination photon or fixed $\boldsymbol{\epsilon}_k$ to a certain direction. But we can invert this situation and, instead of demanding a certain $\boldsymbol{\epsilon}_k$, ask how the emitted recombination radiation is polarized. As a convenient way to mathematically formulate this question we use the so called *Stokes parameters* P_1 and P_2 that characterize the linear polarization of light. These Stokes parameters are quantities that are experimentally easy to access since they are closely related to the intensity I_Φ of the emitted radiation polarized in the angle Φ with respect to the xz-plane. This relation is given by the equations

$$P_1 = \frac{I_{0°} - I_{90°}}{I_{0°} + I_{90°}}, \tag{4.12a}$$

$$P_2 = \frac{I_{45°} - I_{135°}}{I_{45°} + I_{135°}}. \tag{4.12b}$$

Theoretically we can obtain P_1 and P_2 using the relation

$$I_\Phi \propto \left.\frac{\mathrm{d}\sigma^{1s}}{\mathrm{d}\Omega_k}\right|_{\chi=\Phi} \tag{4.13}$$

that tells us that the angle-differential cross section (4.9) with a fixed polarization angle $\chi = \Phi$ is proportional to the intensity I_Φ.

It is common to represent the linear polarization of light in terms of the polarization ellipse which is more figurative than P_1 and P_2. This ellipse is parametrized by

its eccentricity P_{lin} that quantifies the fraction of the emitted radiation that is linearly polarized and the tilt angle χ of its principal axis, which is commonly called *polarization angle*, as shown in Fig. 4.1. The quantities P_{lin} and χ are related to the Stokes parameters via the equations

$$P_{lin} = \sqrt{P_1^2 + P_2^2}, \tag{4.14a}$$

$$\chi = \frac{1}{2} \arctan \frac{P_2}{P_1}. \tag{4.14b}$$

If we apply these equations together with Eq. (4.12) to investigate the polarization of the radiation emitted during the RR process we see immediately from Eq. (4.9) that the parameter P_2 vanishes, while $P_1 = 1$, always. Physically this means that in RR the emitted radiation is completely linearly polarized ($P_{lin} = 1$) within the xz-plane ($\chi = 0$). We will see later that the irradiation of the system "electron-nucleus" with an external laser will lead to a more complicated yet interesting behaviour of P_{lin} and χ than in the case of RR.

Finally we can obtain the total cross section σ^{1s} of RR from the angle-differential cross section by integrating Eq. (4.11) over all directions Ω_k of the photon emission. Thus we arrive at

$$\sigma^{1s} = \frac{2^8 \pi^2}{3c^3} \left(\frac{Z^3}{p(Z^2 + p^2)} \right)^2 \frac{\mathrm{e}^{-4\frac{Z}{p}\operatorname{arccot}\left(\frac{Z}{p}\right)}}{1 - \mathrm{e}^{-2\pi\frac{Z}{p}}}. \tag{4.15}$$

In this equation we see that σ^{1s} can be expressed as a function of Z/p. Therefore it does not change if the ratio between the nuclear charge and the initial electron momentum is kept constant.

4.2 LASER ASSISTED RADIATIVE RECOMBINATION

Having recapitulated the properties of RR, in this section we will derive expressions for the angle-differential and total cross section of LARR. We will discuss the laser assisted recombination of two types of incident electrons. For incoming SCV electrons (2.19) we will obtain expressions for the angle-differential and total cross section and moreover the Stokes parameters of the emitted recombination radiation. In our discussion of LARR with incident Volkov-Bessel electrons (2.15) we will restrict ourselves to the derivation of the angle-differential cross section.

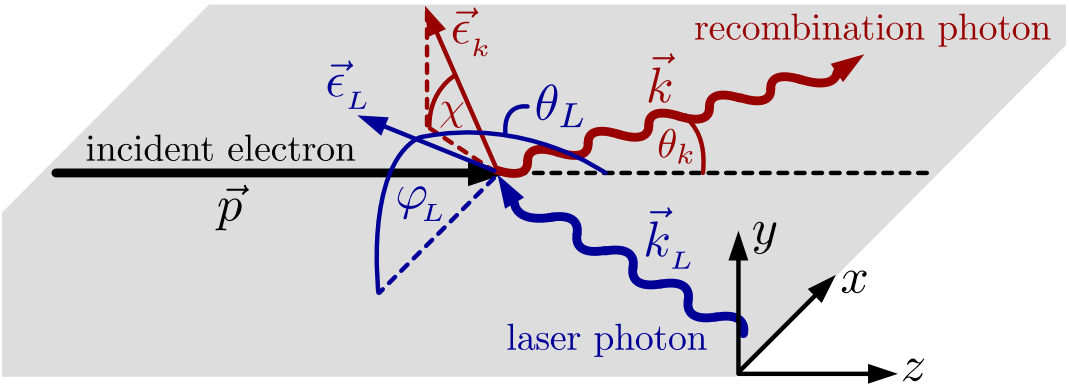

Figure 4.2: Geometry of laser assisted radiative recombination. The z-axis is chosen along the incident electron momentum $\boldsymbol{p}$. The xz-plane is defined by $\boldsymbol{p}$ and the momentum vector of the outgoing photon $\boldsymbol{k}$ whose direction is defined by its polar angle θ_k. The polarization direction of the emitted photon is given by $\boldsymbol{\epsilon}_k$ and characterized by the angle χ while the polarization direction of the external laser $\boldsymbol{\epsilon}_L$ is defined by two angles θ_L and φ_L.

4.2.1 *Geometry*

Due to the external laser the geometry of LARR is similar but slightly more complicated than the one of RR (cf. Fig. 4.1). In Fig. 4.2 we show this geometry again in the rest frame of the atom, where in analogy to Fig. 4.1 the xz-plane is defined by the momentum vectors of the incident electron $\boldsymbol{p}$ and the emitted photon $\boldsymbol{k}$. The direction of the photon emission is given by the angle θ_k while its polarization direction $\boldsymbol{\epsilon}_k$ is defined by the angle χ. We characterize the direction of the external laser by its polarization direction $\boldsymbol{\epsilon}_L$ characterized by the angles θ_L and ϕ_L.

4.2.2 *Laser assisted capture of Coulomb-Volkov electrons*

Making use of the results obtained for RR (cf. Sec. 4.1) in this section we shall derive analytical expressions for the cross section of the laser assisted recombination of SCV electrons (2.19) into the 1s ground state of a hydrogen like ion. In order to arrive at these expressions we need to evaluate the S-matrix (3.7), where the initial state is given by Eq. (2.19) and the final state is given by the laser dressed bound state as shown in Eq. (2.28). Generally we find:

$$\mathcal{S}^{SCV} = -\mathrm{i}\int_{-\infty}^{\infty} \mathrm{d}t \left\langle \widetilde{\psi}_{1s}(\boldsymbol{r},t) \,\middle|\, \mathrm{e}^{\mathrm{i}(\omega_k t - \boldsymbol{k}\cdot\boldsymbol{r})}(\boldsymbol{\epsilon}_k \cdot \nabla) \,\middle|\, \widetilde{\chi}_{\boldsymbol{p}}^{SCV}(\boldsymbol{r},t) \right\rangle . \tag{4.16}$$

Again we employ the dipole approximation ($\boldsymbol{k}\cdot\boldsymbol{r} \ll 1$) for the emitted photon and obtain:

$$\begin{aligned} S^{SCV} = &-\mathrm{i}\int_{-\infty}^{\infty}\mathrm{d}t\int_{\mathbb{R}^3}\mathrm{d}^3\boldsymbol{r}\left[\mathrm{e}^{\mathrm{i}(E_1-E_i+\omega_k)t}\phi_{100}(r)(\boldsymbol{\epsilon}_k\cdot\nabla)\phi_{\boldsymbol{p}}(\boldsymbol{r})\right. \\ &\left.\times\left(\mathrm{e}^{\mathrm{i}\boldsymbol{\alpha}_L(t)\cdot\boldsymbol{p}}+\mathrm{i}\frac{\mathcal{E}_L}{\omega_L}(\boldsymbol{\epsilon}_L\cdot\boldsymbol{r})\cos(\omega_L t)\,\mathrm{e}^{\mathrm{i}\boldsymbol{\alpha}_L(t)\cdot\boldsymbol{p}}\right)\right]. \end{aligned} \tag{4.17}$$

The time integration in the equation above can be performed by making use of the explicit form of $\boldsymbol{\alpha}_L(t)$ and the Jacobi-Anger expansion and its first derivative with respect to t:

$$\mathrm{e}^{\mathrm{i}\kappa\sin(\omega_L t)} = \sum_{N=-\infty}^{\infty}\mathrm{J}_N(\kappa)\,\mathrm{e}^{\mathrm{i}N\omega_L t}, \tag{4.18a}$$

$$\cos(\omega_L t)\,\mathrm{e}^{\mathrm{i}\kappa\sin(\omega_L t)} = \frac{1}{\kappa}\sum_{N=-\infty}^{\infty}N\mathrm{J}_N(\kappa)\,\mathrm{e}^{\mathrm{i}N\omega_L t}, \tag{4.18b}$$

where we defined the abbreviation $\kappa = \mathcal{E}_L(\boldsymbol{\epsilon}_L\cdot\boldsymbol{p})/\omega_L^2$. So the time integrated S-matrix can be written in the form

$$S^{SCV} = 2\pi\mathrm{i}\sum_{N=-\infty}^{\infty}\delta(E_1-E_i+\omega_k-N\omega_L)\mathcal{M}_N^{SCV}(\mathcal{E}_L,\boldsymbol{\epsilon}_L,\boldsymbol{p},Z) \tag{4.19}$$

where the delta function provides for energy conservation which allows us to interpret the *photon number* N as the number of laser photons absorbed ($N>0$) or emitted ($N<0$) by the recombining electron during the interaction with the external laser. Thus the S-matrix decomposes into an infinite number of *partial matrix elements* $\mathcal{M}_N^{SCV}(\mathcal{E}_L,\boldsymbol{\epsilon}_L,\boldsymbol{p},Z)$ each corresponding to a particular number N of exchanged laser photons. These partial matrix elements can be written as a sum of two *constituent matrix elements* $\mathcal{M}_{RR}(\boldsymbol{p},Z)$ and $\mathcal{M}_{dr}(\boldsymbol{p},Z)$:

$$\mathcal{M}_N^{SCV}(\mathcal{E}_L,\boldsymbol{\epsilon}_L,\boldsymbol{p},Z) = \mathrm{J}_N(\kappa)\left(\mathcal{M}_{RR}(\boldsymbol{p},Z)+\frac{N\omega_L}{\boldsymbol{\epsilon}_L\cdot\boldsymbol{p}}\mathcal{M}_{dr}(\boldsymbol{p},Z)\right). \tag{4.20}$$

The first constituent matrix element $\mathcal{M}_{RR}(\boldsymbol{p},Z)$ is the matrix element of laser free recombination (4.8) which we already derived in Sec. 4.1. $\mathcal{M}_{dr}(\boldsymbol{p},Z)$ in contrast has its origin in the dressing contribution to the bound state wave function (2.28). It can be obtained analog to the calculation of $\mathcal{M}_{RR}$ starting with the integral

$$\begin{aligned} \mathcal{M}_{dr}(\boldsymbol{p},Z) &= \int_{\mathbb{R}^3}\mathrm{d}^3\boldsymbol{r}\,(\boldsymbol{\epsilon}_L\cdot\boldsymbol{r})\phi_{100}(\boldsymbol{r})(\boldsymbol{\epsilon}_k\cdot\nabla)\phi_{\boldsymbol{p}}(r) \\ &= -\int_{\mathbb{R}^3}\mathrm{d}^3\boldsymbol{r}\,\phi_{\boldsymbol{p}}(\boldsymbol{r})(\boldsymbol{\epsilon}_k\cdot\nabla)\left[(\boldsymbol{\epsilon}_L\cdot\boldsymbol{r})\phi_{100}(r)\right], \end{aligned} \tag{4.21}$$

where we note that again the surface term vanished after integration by parts. The second line of the equation above can be written in a form very similar to Eq. (4.8):

$$\mathcal{M}_{dr}(\boldsymbol{p}, Z) = -\mathrm{i}2^6\pi^3 B(\boldsymbol{\epsilon}_L \cdot \nabla_k)(\boldsymbol{\epsilon}_k \cdot \nabla_k)\mathcal{I}(\boldsymbol{p}, Z, \boldsymbol{k})\big|_{\boldsymbol{k}=0}. \tag{4.22}$$

Performing the derivations with respect to the components of $\boldsymbol{k}$ we obtain the explicit form of $\mathcal{M}_{dr}(\boldsymbol{p}, Z)$ that reads

$$\mathcal{M}_{dr}(\boldsymbol{p}, Z) = B\left((\boldsymbol{\epsilon}_L \cdot \boldsymbol{\epsilon}_k) - 2(\boldsymbol{\epsilon}_L \cdot \boldsymbol{e}_p)(\boldsymbol{\epsilon}_k \cdot \boldsymbol{e}_p)\frac{2p^2 - \mathrm{i}pZ}{Z^2 + p^2}\right)\frac{\mathrm{e}^{-2\left(\frac{Z}{p} - 2\mathrm{i}\right)\operatorname{arccot}\left(\frac{Z}{p}\right)}}{p(p - \mathrm{i}Z)^3}. \tag{4.23}$$

We will use this expression as well as Eq. (4.8) to express the differential and total cross section of LARR. The photon number interpretation of the expansion index N will allow us to relate the partial matrix elements $\mathcal{M}_N^{SCV}$ to the angle-differential cross section of LARR for the emission of a recombination photon with a particular energy.

4.2.2.1 *Angle-differential cross section*

From the expression we derived for the partial matrix element (4.20) we can define the angle-differential *partial cross section* $\mathrm{d}\sigma_N^{SCV}/\mathrm{d}\Omega_k$ via Eq. (3.10). Physically $\mathrm{d}\sigma_N^{SCV}/\mathrm{d}\Omega_k$ is the cross section for the recombination of an SCV electron that exchanges N photons with the external laser field and recombines into the ground state of a hydrogen like ion. Under the assumption that the polarization of the emitted recombination radiation is not observed we sum over all possible $\boldsymbol{\epsilon}_k$ and obtain for the angle-differential partial cross section using the definition (3.10):

$$\frac{\mathrm{d}\sigma_N^{SCV}}{\mathrm{d}\Omega_k} = \frac{4\pi^2}{c^3 p}\omega_k(N)\sum_{\boldsymbol{\epsilon}_k}\left|\mathcal{M}_N^{SCV}(\mathcal{E}_L, \boldsymbol{\epsilon}_L, \boldsymbol{p}, Z)\right|^2 \tag{4.24}$$

where the frequency $\omega_k(N)$ of the recombination photon is given by the conservation law:

$$\omega_k(N) = E_i - E_1 + N\omega_L. \tag{4.25}$$

Since $\omega_k(N)$ has to be positive, this equation defines a lower limit N_{min} for the photon number due to energy conservation:

$$N \geq N_{min} = \left\lceil \frac{E_1 - E_i}{\omega_L} \right\rceil. \tag{4.26}$$

The angle-differential partial cross section shown in Eq. (4.24) allows us to calculate two important quantities. First the angular distribution of recombination photons with a certain frequency $\omega_k(N)$ and second their energy distribution observed under a certain angle θ_k which we will call the *spectrum* of the emitted photons.

4.2.2.2 *Total cross section*

We can use the expression for the angle-differential cross section $\mathrm{d}\sigma_N^{SCV}/\mathrm{d}\Omega_k$ (4.24) shown above to calculate the corresponding total cross section σ^{SCV}. By integrating Eq. (4.24) over all directions of the photon emission Ω_k and summing over all possible photon numbers N from N_{min} to infinity we obtain:

$$\sigma^{SCV} = \frac{4\pi^2}{c^3 p} \sum_{N=N_{min}}^{\infty} \sum_{\boldsymbol{\epsilon}_k} \int \mathrm{d}\Omega_k \, \omega_k(N) \left| \mathcal{M}_N^{SCV}(\mathcal{E}_L, \boldsymbol{\epsilon}_L, \boldsymbol{p}, Z) \right|^2 . \tag{4.27}$$

Generally the sum over N is semi infinite, but not all terms contribute equally to the total cross section σ^{SCV} (4.27). In fact there is a cut-off photon number N_{cut} beyond which $\mathrm{d}\sigma_N^{SCV}/\mathrm{d}\Omega_k$ drops to zero exponentially. To identify the value of N_{cut} we follow Ref. [45] and perform a stationary phase analysis of the time dependent phase $f(t)$ in Eq. (4.17):

$$f(t) = (E_1 - E_i + \omega_k)t + \boldsymbol{\alpha}_L(t) \cdot \boldsymbol{p}. \tag{4.28}$$

We assume that those terms where $f(t)$ is stationary contribute most to the S-matrix. Therefore we require:

$$\frac{\mathrm{d}f(t)}{\mathrm{d}t} = E_1 - E_i + \omega_k + \frac{E_L}{\omega_L^2}(\boldsymbol{\epsilon}_L \cdot \boldsymbol{p}) \cos(\omega_L t) = 0. \tag{4.29}$$

This equation can be reshaped into the inequality

$$\left| \frac{\omega_k - E_i + E_1}{\omega_L} \right| = \left| \frac{E_L}{\omega_L^2}(\boldsymbol{\epsilon}_L \cdot \boldsymbol{p}) \cos(\omega_L t) \right| \leq \frac{E_L}{\omega_L^2} p. \tag{4.30}$$

Together with the conservation law (4.25) this allows us to calculate the cut-off photon number as

$$N_{cut} = \left\lceil \frac{E_L}{\omega_L^2} p \right\rceil . \tag{4.31}$$

The sharp decay of the partial cross section for photon numbers beyond N_{cut} justifies the formal extension of the summation over N in Eq. (4.27) to negative infinity if $N_{cut} < |N_{min}|$. This possibility will later allow us to derive explicit parametrizations of the total cross section in terms of the laser intensity I_L and frequency ω_L.

4.2.2.3 *Polarization of the emitted photons*

The polarization of the emitted recombination radiation produced by means of LARR can be characterized in the same way as we discussed in Sec. 4.1. The intensity $I_{\Phi,N}(\theta_k)$ of the emitted radiation with polarization angle Φ observed under the angle θ_k with a certain energy determined by N is proportional to the angle-differential partial cross section $\mathrm{d}\sigma_N^{SCV}/\mathrm{d}\Omega_k$

$$I_{\Phi,N}(\theta_k) \propto \frac{4\pi^2}{c^3 p}\omega_k(N)\left|\mathcal{M}_N^{SCV}(\mathcal{E}_L, \boldsymbol{\epsilon}_L, \boldsymbol{p}, Z)\right|^2\Big|_{\chi=\Phi}, \tag{4.32}$$

where, in contrast to Eq. (4.24), we do not sum over all possible $\boldsymbol{\epsilon}_k$ but project on a fixed polarization direction $\chi = \Phi$. In addition we define the energy averaged intensity

$$I_\Phi(\theta_k) = \sum_{N=N_{min}}^{\infty} I_{\Phi,N}(\theta_k), \tag{4.33}$$

which describes the intensity of the emitted recombination radiation under a certain angle θ_k with a fixed polarization angle Φ assuming that the energy of the recombination photons is not observed.

Inserting Eq. (4.32) into Eq. (4.12) we can, using Eq. (4.14), define the degree and direction of linear polarization $P_{lin,N}(\theta_k)$ and $\chi_N(\theta_k)$ of the emitted recombination radiation with a fixed energy and direction. Moreover we can use Eq. (4.33) to obtain $P_{lin}(\theta_k)$ and $\chi(\theta_k)$, being the polarization parameters for the case that the energy of the emitted photons is not measured.

4.2.3 *Laser assisted capture of Volkov-Bessel electrons*

Up to now we discussed the capture of a SCV electron into the ground state of a hydrogen like ion. These SCV electrons behave like a plane wave in the limit of infinite distance between them and the parent atomic nucleus. Volkov-Bessel electrons (2.15) in contrast have a special spacial structure as presented in Fig. 2.1. We will show below how the angle-differential cross section for the laser assisted recombination of such electrons can be obtained. In order to make these results comparable to our calculations for the recombination of SCV electrons, we consider again the capture into the dressed ground state $\widetilde{\psi}_{1s}(\boldsymbol{r}, t)$ (2.28).

First of all we have to note that calculating the S-matrix for LARR using Eq. (2.15) to describe the incident electron comes with a price. We namely neglected the influence of the nucleus on the electron in our derivation of the Volkov-Bessel

wave function $\widetilde{\chi}_{\boldsymbol{p}}^{VB}(\boldsymbol{r},t)$ (2.15), i.e. we applied another approximation beyond what we did in our discussion of SCV electrons. Jaroń *et al.* [19] however have shown that neglecting the Coulomb field of the nucleus is a suitable approximation for high electron energies and high laser intensities. Moreover they found that the qualitative behaviour of their results does not change even for lower energies E_i.

Having the reduced validity of the wave function $\widetilde{\chi}_{\boldsymbol{p}}^{VB}(\boldsymbol{r},t)$ (2.15) in mind we can obtain the S-matrix of LARR for an incident Volkov-Bessel electron by inserting Eqs. (2.11) and (2.28) into Eq. (3.7). It reads in dipole approximation:

$$\begin{aligned}\mathcal{S}^{VB} &= -\mathrm{i}\int_{-\infty}^{\infty}\mathrm{d}t\,\left\langle \widetilde{\psi}_{1s}(\boldsymbol{r},t)\,\middle|\,\mathrm{e}^{\mathrm{i}\omega_k t}(\boldsymbol{\epsilon}_k\cdot\nabla)\,\middle|\,\widetilde{\chi}_{\boldsymbol{p}}^{VB}(\boldsymbol{r},t)\right\rangle \\ &= \int_0^{\infty}\mathrm{d}p_\perp\int_0^{2\pi}\mathrm{d}\varphi_p\,\delta(p_\perp-\varkappa)p_\perp\frac{\mathrm{e}^{\mathrm{i}l\varphi_p}}{2\pi\mathrm{i}^l\varkappa}\mathcal{S}^V,\end{aligned} \tag{4.34}$$

where $\mathcal{S}^V$ is the S-matrix for the laser assisted capture of a single Volkov electron (2.9). It is noteworthy that the $\mathcal{S}^{VB}$ (4.34) is obtained by superimposing S-matrices for plane-wave-like incident electrons $\mathcal{S}^V$ in the same way we integrated over plane-wave-like wave functions to obtain the Volkov-Bessel state (cf. Eq. (2.15)).

The S-matrix $\mathcal{S}^V$ for the recombination of a single Volkov electron takes a form similar to Eq. (4.17):

$$\mathcal{S}^V = 2\pi\mathrm{i}\sum_{N=-\infty}^{\infty}\delta(E_1-E_i+\omega_k-N\omega_L)\mathcal{M}_N^V(\mathcal{E}_L,\boldsymbol{\epsilon}_L,\boldsymbol{p},Z), \tag{4.35}$$

where the partial matrix element $\mathcal{M}_N^V(\mathcal{E}_L,\boldsymbol{\epsilon}_L,\boldsymbol{p},Z)$ again splits up into two constituent matrix elements in the same way as shown in Eq. (4.20). With the relations given in Ref. [35] we obtain the closed form of these matrix elements:

$$\mathcal{M}_{RR}^V(\boldsymbol{p},Z) = \frac{2}{\pi}\sqrt{2Z^5}\frac{\boldsymbol{\epsilon}_k\cdot\boldsymbol{p},}{(p^2+Z^2)^2} \tag{4.36a}$$

$$\mathcal{M}_{dr}^V(\boldsymbol{p},Z) = \mathrm{i}\frac{2^3}{\pi}\sqrt{2Z^5}\frac{(\boldsymbol{\epsilon}_L\cdot\boldsymbol{p})(\boldsymbol{\epsilon}_k\cdot\boldsymbol{p})}{(p^2+Z^2)^2}. \tag{4.36b}$$

Here $\mathcal{M}_{RR}^V(\boldsymbol{p},Z)$ again characterizes the laser free RR, while $\mathcal{M}_{dr}^V(\boldsymbol{p},Z)$ describes the contribution to the matrix element $\mathcal{M}_N^V(\mathcal{E}_L,\boldsymbol{\epsilon}_L,\boldsymbol{p},Z)$ that arises due to the laser dressing of the bound state.

To get an explicit expression for the S-matrix $\mathcal{S}^{VB}$ (4.34) shown above in a general shape, we need to perform the integration over the transverse electron momentum $\boldsymbol{p}_\perp$. The integration over the radial component $p_\perp$ is readily performed by taking $\mathcal{S}^V$ (4.35) at $p_\perp = \varkappa$, while we integrate numerically over the azimutal angle φ_p.

Eventually the partial matrix element for the recombination for a Volkov-Bessel electron can be written as:

$$\mathcal{M}_N^{VB}(\mathcal{E}_L, \boldsymbol{\epsilon}_L, \boldsymbol{p}, Z) = \int_0^{2\pi} \mathrm{d}\varphi_p \, \frac{\mathrm{e}^{\mathrm{i}l\varphi_p}}{2\pi \mathrm{i}^l} \, \mathcal{M}_N^V(\mathcal{E}_L, \boldsymbol{\epsilon}_L, \boldsymbol{p}, Z)\Big|_{p_\perp = \varkappa}. \tag{4.37}$$

Because of the spatial structure of the incident Volkov-Bessel electron this equation is not general. It describes the recombination process for a single target ion placed in the center of the incoming electron beam. To describe LARR for arbitrary distances between the target ion and the beam axis we have to parallel shift the Volkov-Bessel electron beam along a vector $\boldsymbol{b}_\perp$ away from the z-axis. We commonly call $\boldsymbol{b}_\perp$ *impact paramter*. The parallel shift is performed by acting with the translation operator $\exp(\boldsymbol{b}_\perp \cdot \hat{\boldsymbol{p}})$ on the wave function of the initial Volkov-Bessel electron. Because the wave function $\widetilde{\chi}_{\boldsymbol{p}}^{VB}(\boldsymbol{r}, t)$ is an eigenfunction of the momentum operator $\hat{\boldsymbol{p}}$ with eigenvalue $\boldsymbol{p}$ we obtain for the S-matrix $\mathcal{S}^{VB}$ for a non-zero impact parameter:

$$\mathcal{S}^{VB}(\boldsymbol{b}_\perp) = \int_0^\infty \mathrm{d}p_\perp \int_0^{2\pi} \mathrm{d}\varphi_p \, \delta(p_\perp - \varkappa) p_\perp \frac{\mathrm{e}^{\mathrm{i}l\varphi_p}}{2\pi \mathrm{i}^l \varkappa} \, \mathrm{e}^{\mathrm{i}\boldsymbol{b}_\perp \cdot \boldsymbol{p}} \mathcal{S}^V, \tag{4.38}$$

with the corresponding matrix element

$$\mathcal{M}_N^{VB}(\boldsymbol{b}_\perp, \mathcal{E}_L, \boldsymbol{\epsilon}_L, \boldsymbol{p}, Z) = \int_0^{2\pi} \mathrm{d}\varphi_p \, \frac{\mathrm{e}^{\mathrm{i}l\varphi_p}}{2\pi \mathrm{i}^l} \, \mathrm{e}^{\mathrm{i}\boldsymbol{b}_\perp \cdot \boldsymbol{p}} \, \mathcal{M}_N^V(\mathcal{E}_L, \boldsymbol{\epsilon}_L, \boldsymbol{p}, Z)\Big|_{p_\perp = \varkappa}. \tag{4.39}$$

We will later use the expressions above to describe the laser assisted recombination of Volkov-Bessel electrons with targets that are much larger than the diameter of the incident electron beam. For that purpose we will perform an integration over the impact parameter to account for the interaction between the electron and the whole target.

4.2.3.1 *Angle-differential cross section*

We can calculate the angle-differential cross section of LARR for the case of an incident Volkov-Bessel electron in analogy to Eq. (4.24) using Eqs. (4.34) and (4.38). For $\boldsymbol{b}_\perp = 0$ we find the angle-differential partial cross section

$$\frac{\mathrm{d}\sigma_N^{VB}}{\mathrm{d}\Omega_k} = \left| \int_0^{2\pi} \mathrm{d}\varphi_p \, \frac{\mathrm{e}^{\mathrm{i}l\varphi_p}}{2\pi \mathrm{i}^l} \, \mathcal{M}_N^V(\mathcal{E}_L, \boldsymbol{\epsilon}_L . \boldsymbol{p}, Z)\Big|_{p_\perp = \varkappa} \right|^2. \tag{4.40}$$

If in contrast we assume that the target is a dilute target (i.e. there is no interaction between the target atoms) much larger than the extent of the incoming electron

beam we have to integrate over the impact parameter $\boldsymbol{b}_\perp$. Thus for the *target averaged* angle-differential partial cross section we find:

$$\begin{aligned}\overline{\frac{\mathrm{d}\sigma_N^{VB}}{\mathrm{d}\Omega_k}} = \int_{\mathbb{R}^2} \mathrm{d}^2\boldsymbol{b}_\perp \int_0^{2\pi} \mathrm{d}\varphi_p \int_0^{2\pi} \mathrm{d}\varphi_p' \, \frac{\mathrm{e}^{\mathrm{i}l(\varphi_p - \varphi_p')}}{4\pi^2} \, \mathrm{e}^{\mathrm{i}\boldsymbol{b}_\perp \cdot (\boldsymbol{p} - \boldsymbol{p}')} \\ \times \, \mathcal{M}_N^V(\mathcal{E}_L, \boldsymbol{\epsilon}_L, \boldsymbol{p}, Z)\Big|_{p_\perp = \varkappa} \, \mathcal{M}_N^V(\mathcal{E}_L, \boldsymbol{\epsilon}_L, \boldsymbol{p}', Z)^*\Big|_{p_\perp' = \varkappa},\end{aligned} \tag{4.41}$$

where the integration over the impact parameter can be directly performed resulting in a factor $2\pi\delta^{(3)}(\boldsymbol{p} - \boldsymbol{p}')$. Therefore the target averaged cross section can be written as

$$\overline{\frac{\mathrm{d}\sigma_N^{VB}}{\mathrm{d}\Omega_k}} = \int_0^{2\pi} \frac{\mathrm{d}\varphi_p}{2\pi} \left| \mathcal{M}_N^V(\mathcal{E}_L, \boldsymbol{\epsilon}_L, \boldsymbol{p}, Z)\Big|_{p_\perp = \varkappa} \right|^2 . \tag{4.42}$$

The equation above shows that the target averaging wipes out all dependencies on the orbital angular momentum l of the incident electron. This is an effect that has been already seen in previous works for the interaction of atomic systems with twisted electrons [35] and similarly for twisted photons [46, 47]. If the energy of the emitted recombination photon is not observed we obtain the N-independent angle-differential cross section $\overline{\mathrm{d}\sigma^{VB}}/\mathrm{d}\Omega_k$ in analogy to Eqs. (4.27) and (4.33) by summing over all possible photon numbers.

5 RESULTS AND DISCUSSION

In chapter 4 we developed a theory do describe the laser assisted recombination of an electron into the ground state of a hydrogen like ion. There we considered two different wave functions for the incident electrons. First an approximate solution of the TDSE with Hamiltonian (2.16) describing an electron in the superposition of the atomic potential and the vector potential of the external laser. And secondly we superimposed Volkov wave functions (2.9) in such a way that the resulting Volkov-Bessel wave function (2.15) has a certain orbital angular momentum and a Bessel-like intensity profile. For both types of incident electrons we derived expressions for the angle-differential cross section and in the case of an incoming Coulomb-Volkov electron (2.19) we moreover got the total cross section. And were able to describe the polarization of the emitted recombination photons. In this chapter we will first discuss results for the differential and total cross section of LARR where the incoming electron is described by a SCV wave function (2.19) and afterwards we will compare these findings with calculations performed for incident Volkov-Bessel electrons.

5.1 RECOMBINATION OF COULOMB-VOLKOV ELECTRONS

In this section we will discuss the laser assisted recombination of SCV continuum electrons (2.19) into the ground state of hydrogen like ions, described by a perturbatively laser dressed bound state wave function (2.28). We will focus our study on the influence of the laser parameters on the cross section of LARR and on the effects arising due to the laser dressing of the bound state.

5.1.1 *Angular and energy distribution of the emitted photons*

We start our discussion of LARR for incident SCV electrons with results for the angle-differential partial cross section $\mathrm{d}\sigma_N^{SCV}/\mathrm{d}\Omega_k$ (4.24). From $\mathrm{d}\sigma_N^{SCV}/\mathrm{d}\Omega_k$ (4.24) we can calculate the energy distribution of the emitted recombination photons by fixing the photon emission angle θ_k and calculating $\mathrm{d}\sigma_N^{SCV}/\mathrm{d}\Omega_k$ as a discrete function of the recombination photon energy $\omega_k(N)$ (4.25). We will refer to this discrete function as the *spectrum* of the recombination photons. Fig. 5.1 shows this

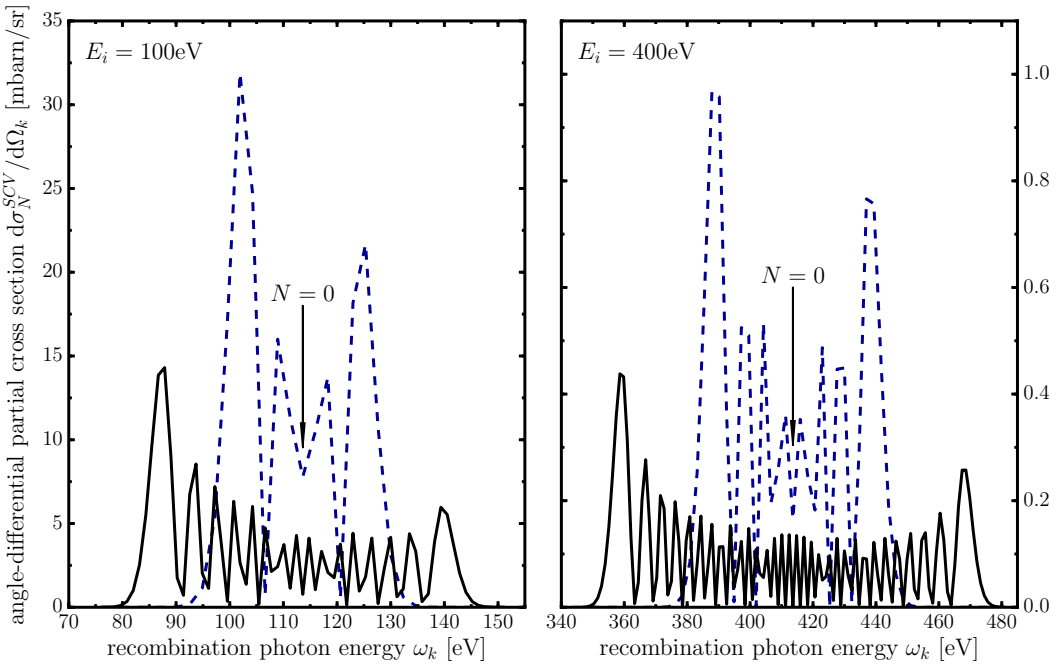

Figure 5.1: Energy distribution of the emitted recombination photons for $Z = 1$ and two different initial electron energies $E_i = 100\,\mathrm{eV}$ (left panel) and $E_i = 400\,\mathrm{eV}$ (right panel) and two laser photon energies $\omega_L = 1.17\,\mathrm{eV}$ (black solid lines) and $\omega_L = 2.34\,\mathrm{eV}$ (blue dashed lines). The calculations have been performed for a laser with intensity and polarization $I_L = 10^{13}\,\mathrm{W/cm^2}$ and $\theta_L = \varphi_L = 0°$, respectively. The photon emission angle is fixed to $\theta_k = 45°$.

spectrum for two incident electron energies $E_i = 100\,\mathrm{eV}$ (left panel) and $E_i = 400\,\mathrm{eV}$ (right panel) and two laser photon energies ω_L. The laser polarization is chosen parallel to the direction of the incident electron ($\theta_L = \phi_L = 0$). Although the spectrum is discrete and only defined at the energies $\omega_k(N)$ (4.25), we plot our results as lines to guide the eye. In the case of laser-free radiative recombination the emitted photons are monochromatic and their energy is given by the energy conservation law $\omega_k = E_i - E_1$. As seen in Fig. 5.1 this is not the case if the electron and the ion are exposed to an external laser. The spectrum of photons emitted during the process of LARR has a plateau-like shape with sharp cut offs giving the spectrum a well defined width. The loci of these cut offs are given by Eq. (4.25) at $N = \pm N_{cut}$, where the cut off photon number N_{cut} is shown in Eq. (4.31). Comparing both panels of Fig. 5.1 we see that the spectrum is very sensitive to the incident electron energy E_i. For higher E_i the width of the spectrum is increased,

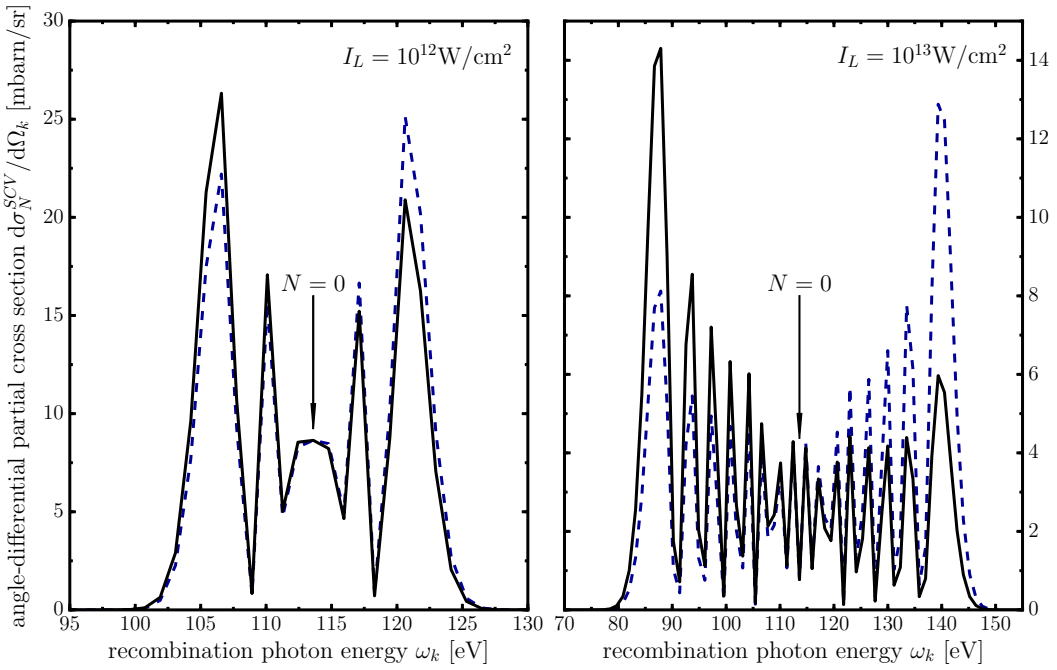

Figure 5.2: Angle-differential partial cross section (4.24) for the laser assisted recombination of a $E_i = 100\,\mathrm{eV}$ electron and a hydrogen nucleus ($Z = 1$) as a function of the recombination photon energy $\omega_k(N)$. The calculations have been performed for a photon emission angle $\theta_k = 45°$ and a laser polarization $\theta_L = \varphi_L = 0°$. The laser parameters are $\hbar\omega_L = 1.17\,\mathrm{eV}$, $I_L = 10^{12}\,\mathrm{W/cm^2}$ (left panel) and $I_L = 10^{13}\,\mathrm{W/cm^2}$ (right panel). The black solid lines represent the full calculations, the blue dashed lines refer to the results where the dressing of the target bound states is neglected.

while the probability of the process as whole is suppressed. An increasing laser photon energy ω_L has the reverse effect, which we can also deduce from Eq. (4.31).

We have seen that the spectrum of LARR is strongly affected by the external laser. Below we will isolate the effects on the spectrum that arise from the influence of the external laser on the residual bound state. Therefore we recall that the constituent Matrix element $\mathcal{M}_{dr}(\boldsymbol{p}, Z)$ (4.23) originates *only* from the bound state dressing. Therefore it is straightforward to obtain results for undressed bound states by setting $\mathcal{M}_{dr}(\boldsymbol{p}, Z) = 0$. Fig. 5.2 shows such results for the recombination of a $E_i = 100\,\mathrm{eV}$ electron into the ground state of hydrogen, obtained under the assumption that the final bound state is not influenced by the external laser. For comparison the corresponding full calculations are shown. The results have

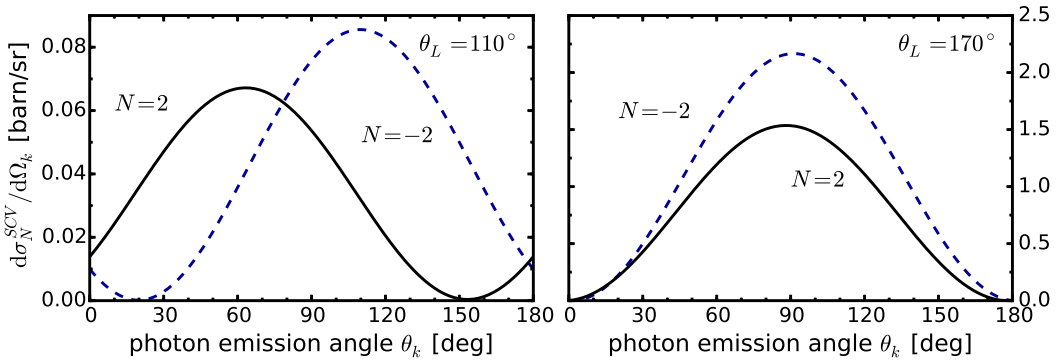

Figure 5.3: Angle-differential partial cross section (4.24) for the laser assisted recombination of a $E_i = 15\,\text{eV}$ electron and a hydrogen nucleus ($Z = 1$) as a function of the photon emission angle θ_k. The calculations have been performed for two directions of the laser polarization $\theta_L = 110^\circ$ (left panel) and $\theta_L = 170^\circ$ (right panel) in a coplanar setup ($\varphi_L = 0^\circ$) and two different photon numbers $N = -2$ (blue dashed lines) and $N = 2$ (black solid lines). The laser parameters are $\hbar\omega_L = 2.34\,\text{eV}$ and $I_L = 10^{13}\,\text{W/cm}^2$.

been obtained for two different laser intensities $I_L = 10^{12}\,\text{W/cm}^2$ (left panel) and $I_L = 10^{13}\,\text{W/cm}^2$ (right panel) and the laser photon energy $\hbar\omega_L = 1.17\,\text{eV}$. The photon emission angle is fixed to $\theta_k = 45^\circ$ and the laser polarization is chosen parallel to the quantization (z-) axis. We see in Fig. 5.2 that the "dressed" and "undressed" results indeed have the same spectral width but nevertheless a qualitatively different shape. The spectra obtained for undressed bound states are symmetric around the field-free recombination photon energy, where $N = 0$. The slight increase of $d\sigma_N^{SCV}/d\Omega_k$ towards higher values of $\omega_k(N)$ arises due to the prefactor $\omega_k(N)$ in Eq. (4.24). The calculations with dressed bound state wave functions, in contrast, exhibit a strong asymmetry, especially for the outer sidebands of the spectrum, where the photon number N is large. This can be explained by the fact that the contribution of $\mathcal{M}_{dr}(\boldsymbol{p}, Z)$ increases with N, therefore the asymmetries are the strongest for large photon numbers. But these strong asymmetries can only be observed if the intensity of the external laser is sufficiently high because otherwise sidebands corresponding to larger photon numbers are not visible (cf. Eq. (4.31)).

Up to now we have discussed the spectrum of the emitted recombination photons where we fixed the direction of the photon emission. We can turn the situation and calculate the angular distribution of the recombination photons given by $d\sigma_N^{SCV}/d\Omega_k$ as a function of θ_k but now for a fixed recombination photon energy $\omega_k(N)$. In case of laser free RR this angular distribution is proportional to $\sin^2\theta_k$ and hence symmetric around $\theta_k = 90^\circ$ (cf. Sec. 4.1). In Fig. 5.3 we see that for the

case of LARR $\mathrm{d}\sigma_N^{SCV}/\mathrm{d}\Omega_k$ still has a shape similar to $\sin^2\theta_k$ but the maximum is shifted away from $\theta_k = 90°$. This asymmetric shift becomes the larger the more the laser polarization deviates from the direction of the incident electron momentum $\boldsymbol{p}$, the cross section however is decreased in that case. We can interpret this from a classical point of view. If the electron interacts with a laser field it gets accelerated along the direction of the laser polarization. Therefore its propagation direction at the moment of recombination differs from $\boldsymbol{p}$ which is reflected in a shift of the emission maximum of the angular distribution. As seen from the figure, the direction of the shift depends on the sign of the photon number N. Moreover we find that absorbing a certain number of photons decreases the cross section while emitting the same number of photons makes the recombination more probable. This is an observation that can be made similarly already in the laser-free RR case, where the cross section is increased for lower incident electron energies.

Besides the influence of the laser polarization direction on the angular distribution in Fig. 5.4 we will compare again results obtained for the case where we neglected the laser influence on the residual bound state (dashed lines) with calculations where we did not (solid lines). As seen from the figure the emission pattern of the recombination photons is symmetric around $\theta_k = 90°$ if the bound state dressing is not taken into account. This behaviour is easily understood by setting $\mathcal{M}_{dr}(\boldsymbol{p}, Z) = 0$ in Eq. (4.20). The LARR cross section depends then only on the RR matrix element $\mathcal{M}_{RR}(\boldsymbol{p}, Z)$ weighted with a Bessel function. Therefore the shape of the angular distribution is not altered by the external laser if the bound state dressing is neglected. A different angular behaviour occurs if $\mathcal{M}_{dr}(\boldsymbol{p}, Z)$ is included in the calculations. In that case additional angular dependent terms contribute to the angular distribution leading to an asymmetric shift as already seen in Fig. 5.3. Due to the prefactor of $\mathcal{M}_{dr}(\boldsymbol{p}, Z)$ in Eq. (4.20) this shift becomes the larger the more photons are exchanged between the electron and the laser field. The visibility of large asymmetries however, corresponding to large N, is again restricted by the cut off N_{cut}. In order to observe considerable shifts of the angular distribution therefore either I_L or E_i have to be sufficiently high.

5.1.2 *Polarization of the emitted radiation*

In Ch. 4 we have already seen that the angle-differential cross section can be used to calculate the polarization of the emitted recombination radiation. For the case of laser free RR this radiation is completely linearly polarized within the xz-plane due to the planar symmetry of the process (cf. Sec. 4.1). If we consider LARR instead of RR this symmetry is broken by the external laser field and we therefore

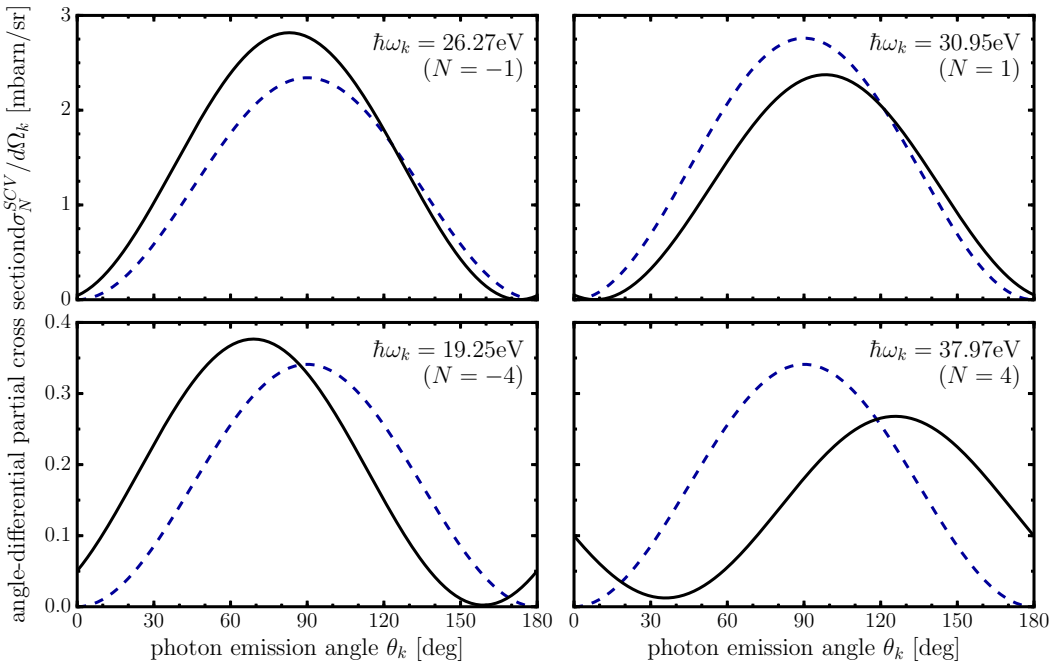

Figure 5.4: Angle-differential partial cross section (4.24) for the laser assisted recombination of a $E_i = 15\,\text{eV}$ electron into the ground state of hydrogen ($Z = 1$) as a function of the photon emission angle θ_k. The assisting laser has an intensity of $I_L = 10^{13}\,\text{W/cm}^2$ and a laser photon energy $\hbar\omega_L = 2.34\,\text{eV}$. Its polarization angles are $\theta_L = 60°$ and $\phi_k = 0°$. Results are shown for four different recombination photon energies; in the upper row $\hbar\omega_k(N = -1) = 26.27\,\text{eV}$ (left panel) and $\hbar\omega_k(N = 1) = 30.95\,\text{eV}$ (right panel) while in the lower row $\hbar\omega_k(N = -4) = 19.25\,\text{eV}$ (left panel) and $\hbar\omega_k(N = 4) = 37.97\,\text{eV}$ (right panel). In all panels we show in comparison results including (black solid lines) and omitting (blue dashed lines) the bound state dressing.

expect that the polarization of the emitted radiation is sensitive to the direction of the laser polarization.

Fig. 5.5 shows the degree of linear polarization P_{lin} (upper row) and the polarization angle χ (lower row) as a function of the azimutal laser polarization angle φ_L for two incident electron energies $E_i = 50\,\text{eV}$ (left column) and $E_i = 100\,\text{eV}$ (right column). The calculations have been performed for a fixed photon emission angle $\theta_k = 175°$ and three different polar laser polarization angles $\theta_k = 30°$ (black solid lines), $\theta_k = 60°$ (blue dashed lines) and $\theta_k = 90°$ (red dotted lines). All results are obtained under the assumption that the energy of the emitted photons is not observed. In Fig. 5.5 we see that the recombination radiation is completely linearly

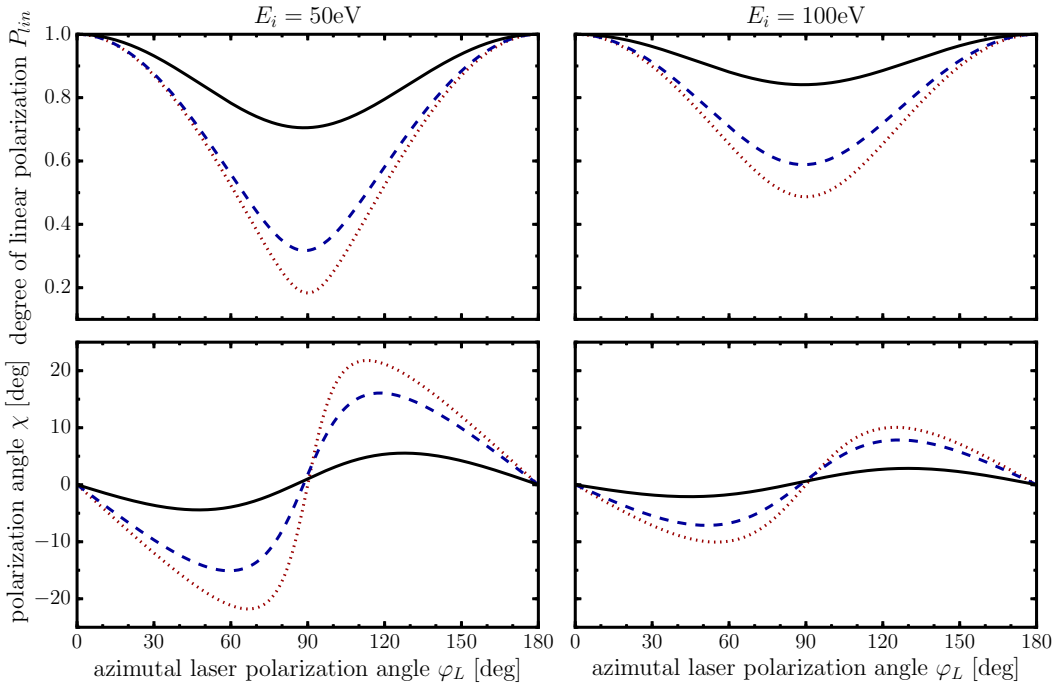

Figure 5.5: Degree of linear polarization P_{lin} (upper row) and polarization angle χ (lower row) of the radiation emitted during the recombination of $E_i = 50\,\text{eV}$ (left column) and $E_i = 100\,\text{eV}$ (left column) electrons into the 1s state of a hydrogen nucleus ($Z = 1$) as a function of the azimutal laser polarization angle φ_L. The laser parameters are $I_L = 10^{13}\,\text{eV}$ and $\omega_L = 2.34\,\text{eV}$. The calculations have been performed for a fixed photon emission angle $\theta_k = 175°$ and three different polar laser polarization angles $\theta_L = 30°$ (black solid lines), $\theta_L = 60°$ (blue dashed lines) and $\theta_L = 90°$ (red dotted lines).

polarized ($P_{lin} = 1$) within the xz-plane ($\chi = 0$) if the geometry of the process is coplanar, i.e. if the laser is polarized within the xz-plane. This is the same behaviour we would expect from laser free radiative recombination. However, if the laser polarization is rotated out of the xz-plane the emitted recombination radiation depolarizes to a minimal value at $\varphi_L = 90°$. This minimum becomes the more pronounced, the more the polar laser polarization angle θ_L approaches 90°. The polarization angle χ is also affected by the variation of φ_L. In contrast to the case of RR, where χ is always zero it can reach values of more than $\chi = 20°$ for LARR. Moreover it can be seen from Fig. 5.5, that the effect of the external laser on the polarization of the recombination radiation becomes weaker if the incident electron energy is increased. While the radiation can depolarize to less than $P_{lin} = 0.2$ for

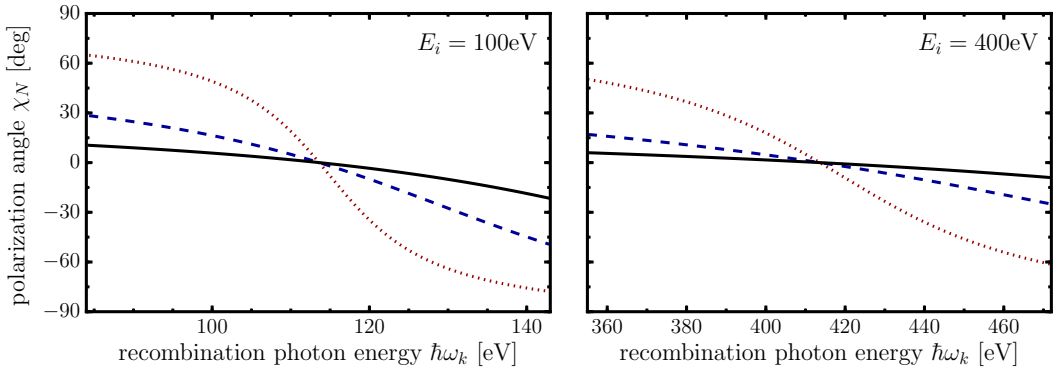

Figure 5.6: Polarization angle χ_N of the emitted recombination radiation as a function of the recombination photon energy $\hbar\omega_k(N)$. The calculations have been performed for $Z = 1$ and a $I_L = 10^{13}\,\mathrm{W/cm^2}$ laser with $\omega_L = 1.17\,\mathrm{eV}$. The direction of the laser polarization is given by $\theta_L = 60°$ and $\varphi_L = 90°$. In both panels results are shown for three different photon emission angles $\theta_k = 90°$ (black solid lines), $\theta_k = 20°$ (blue dashed lines) and $\theta_k = 5°$ (red dotted lines). The left panel shows results for $E_i = 100\,\mathrm{eV}$ while in the right panel $E_i = 400\,\mathrm{eV}$.

$E_i = 50\,\mathrm{eV}$ the minimal degree of linear polarization for $E_i = 100\,\mathrm{eV}$ is $P_{lin} = 0.5$. A similar observation can be made for the polarization angle χ. It reaches $\chi = 20°$ for $E_i = 50\,\mathrm{eV}$ but only $\chi = 10°$ for $E_i = 100\,\mathrm{eV}$.

The results shown in Fig. 5.5 illustrated how the polarization of the emitted recombination radiation depends on the polarization direction of the external laser. But in addition to that in the previous section we have seen that the angle-differential partial cross section $\mathrm{d}\sigma_N^{SCV}/\mathrm{d}\Omega_k$ of LARR may also strongly depend on the energy of the emitted photon parametrized by the number N of exchanged laser photons. As the polarization angle χ_N is calculated from this cross section we also expect a dependence here. Therefore in Fig. 5.6 we show χ_N as a function of the recombination photon energy $\hbar\omega_k(N)$ for two incident electron energies $E_i = 100\,\mathrm{eV}$ (left panel) and $E_i = 400\,\mathrm{eV}$ (right panel). The calculations have been performed for a fixed direction of the laser polarization $\theta_L = 60°$ and $\varphi_L = 90°$ and three photon emission angles $\theta_k = 90°$ (black solid lines), $\theta_k = 20°$ (blue dashed lines) and $\theta_k = 5°$ (red dotted lines). However, the results are discrete again we show a continuous line to guide the eye. Again we see from Fig. 5.6 that the effect of the external laser on the polarization of the emitted recombination radiation is weaker if the energy of the incident electron is increased. Moreover the direction of polarization rotates depending on the number of exchanged laser photons. The rotation becomes the larger the more photons are exchanged with the laser field,

i.e. the larger N is. For a decreasing photon emission angle θ_k the polarization angle can even exceed $\chi = -65°$. This is an observation that has been made similarly in the process of laser assisted Compton scattering [45], where the authors found that the Stokes parameter P_2 varies with increasing N.

5.1.3 *Total cross section: Energy, frequency and intensity scaling*

Up to now we have discussed the differential cross section of LARR and, as a related quantity, the polarization of the emitted recombination radiation. We have seen that the differential partial cross section is very sensitive to the photon number N. As the maximal photon number N_{cut} (4.31) depends on the initial electron energy E_i, the laser frequency ω_L and the laser electric field strength E_L (and thus the laser intensity I_L), we expect differences between the total cross section of RR and LARR as a function of these quantities. The considerations below will focus on this comparison between the laser free and the laser assisted process.

Before we discuss numerical results we briefly look again at the analytical formula for the total LARR cross section σ^{SCV} as shown in Eq. (4.27). For all scenarios discussed below the condition $N_{cut} < |N_{min}|$ is satisfied so we can, in a very good approximation, extend the summation over the photon number N to negative infinity. In this case the infinite sum in Eq. (4.27) converges to the following relations:

$$\sum_{N=-\infty}^{\infty} \mathrm{J}_N^2(\kappa) = 1, \tag{5.1a}$$

$$\sum_{N=-\infty}^{\infty} N^2 \mathrm{J}_N^2(\kappa) = \frac{\kappa^2}{2}, \tag{5.1b}$$

$$\sum_{N=-\infty}^{\infty} N^{2j+1} \mathrm{J}_N^2(\kappa) = 0 \text{ for } j \in \mathbb{N}_0. \tag{5.1c}$$

$$\tag{5.1d}$$

The total cross section can be written then in the following form:

$$\begin{aligned} \sigma^{SCV} =& \frac{4\pi^2}{c^3 p} \sum_{\epsilon_k} \int \mathrm{d}\Omega_k \left\{ (E_i - E_1) |\mathcal{M}_{RR}|^2 \right. \\ &\left. + \frac{\mathcal{E}_L^2}{2\omega_L^2} \left[(E_i - E_1) |\mathcal{M}_{dr}|^2 + (\boldsymbol{\epsilon}_L \cdot \boldsymbol{p}) \mathrm{Re}(\mathcal{M}_{RR}^* \mathcal{M}_{dr}) \right] \right\}. \end{aligned} \tag{5.2}$$

This equation splits into three terms. The first term is the total cross section σ^{1s} of laser free RR as shown in Eq. (4.15). The other two terms share the prefactor

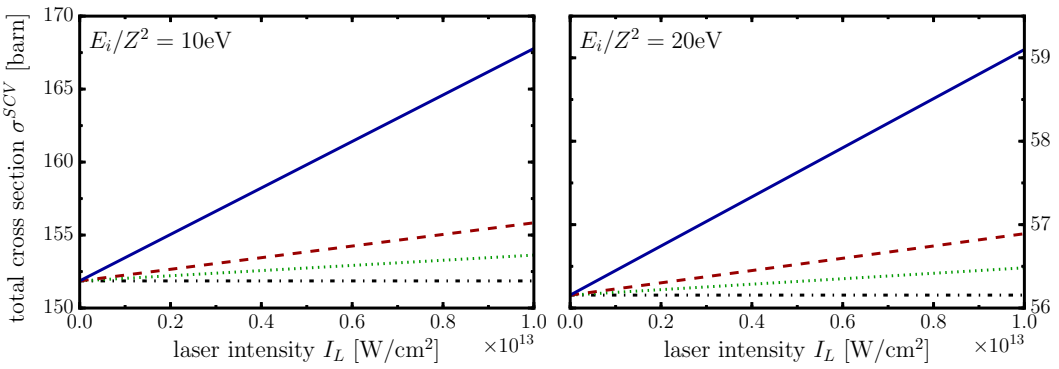

Figure 5.7: Total cross section for laser assisted radiative recombination into the ground state of a hydrogen-like ion as a function of the laser intensity I_L for $\omega_L = 1.17\,\text{eV}$ and three different nuclear charges ($Z = 1$: blue solid line; $Z = 2$; red dashed line; $Z = 3$: green dotted line). The initial electron energy is normalized with respect to the nuclear charge such that $E_i/Z^2 = 10\,\text{eV}$ (left panel) and $E_i/Z^2 = 20\,\text{eV}$ (right panel). The laser polarization is given by $\theta_L = 90°$ and $\varphi_L = 0°$. For comparison the laser free case, respectively the result obtained with an undressed bound state wave functions is shown (black dash-dotted line).

$\mathcal{E}_L^2/(2\omega_L^2)$ that sets the parametric scaling of σ^{SCV}. While the second term is the module squared of the dressing matrix element $\mathcal{M}_{dr}$ the contributions of RR and laser dressing are mixed in the last addend. The influence of this mixing on σ^{SCV} depends on the direction of the laser polarization and vanishes completely if $\boldsymbol{\epsilon}_L$ is perpendicular to $\boldsymbol{p}$. Of course equation (5.2) shows the proper behaviour in the limit vanishing field strength $\mathcal{E}_L \to 0$ and reduces to the cross section of laser free RR. But there is a second limit with the identical result. If we set $\mathcal{M}_{dr} = 0$ all dependencies on the external laser field vanish and σ^{SCV} (5.2) turns into σ^{1s} (4.15). Therefore all influence of the external laser on the total cross section of LARR origins from the laser dressing of the final bound state.

In addition to its RR and non-dressing limit we can see from Eq. (5.2) that the total cross section scales quadratically with the laser electric field amplitude $\mathcal{E}_L$ and therefore linearly with the intensity I_L. This behaviour can be also seen in Fig. 5.7, where we show the laser free ("undressed") cross section in comparison to the total cross section σ^{SCV} as a function of the laser intensity I_L for three different nuclear charges Z. Moreover we present the results that we obtained with the aid of Eq. (4.27), for two sets of initial electron energies $E_i = 10\,\text{eV} \cdot Z^2$ and $E_i = 20\,\text{eV} \cdot Z^2$. This normalization of E_i with respect to Z is applied to separate off the Z-scaling of the laser free RR cross section σ^{1s} (4.15) which is solely defined by the Sommerfeld

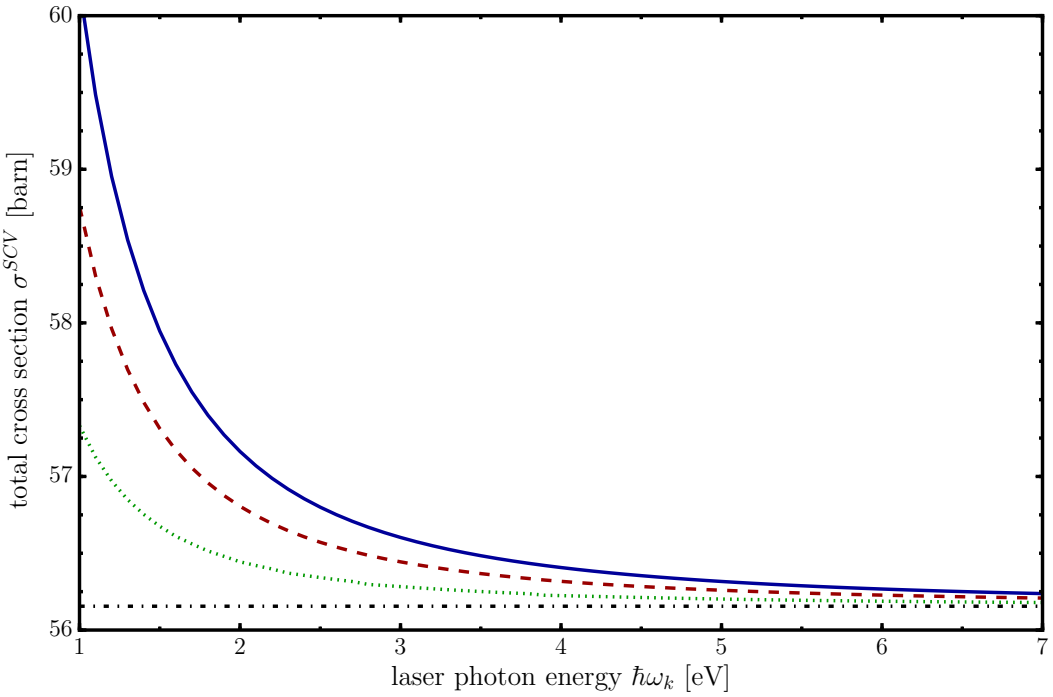

Figure 5.8: Total cross section for the laser assisted radiative recombination of a $E_i = 20\,\mathrm{eV}$ electron into the ground state of a hydrogen ($Z = 1$) ion as a function of the laser frequency ω_L and $I_L = 10^{13}\,\mathrm{W/cm^2}$. The calculations have been performed for $\phi_L = 0°$ and three different polar laser polarization angles $\theta_L = 90°$ (blue solid line), $\theta_L = 60°$ (red dashed line) and $\theta_L = 45°$ (green dotted line). For comparison the laser free case, respectively the result obtained with undressed bound state wave functions is shown (black dash-dotted line).

parameter $\nu = \sqrt{Z^2/(2E_i)}$ and, hence, does not change if E_i/Z^2 is kept constant. Therefore all deviations between the results for different Z shown in Fig. 5.7 arise due to the external laser and in particular the dressing of the residual bound state. We see in Fig. 5.7 that the slope σ^{SCV} as a function of I_L becomes smaller if Z is increased. This occurs due to the stronger binding of the electron in the ground state of the hydrogen like ion for higher Z. Moreover it can be seen again that the influence of the external laser is reduced if the incident electron energy is higher.

The second parametric dependence of the total cross section, that can be read off Eq. (5.2) is the scaling of σ^{SCV} with ω_L. This dependence is shown in Fig. 5.8 where we calculated σ^{SCV} as a function of ω_L for three different polar laser polarization angles θ_L and $\varphi_L = 0$. Our calculations performed with the aid of Eq. (4.27) reflect the expected scaling of the total cross section with the inverse square of the laser

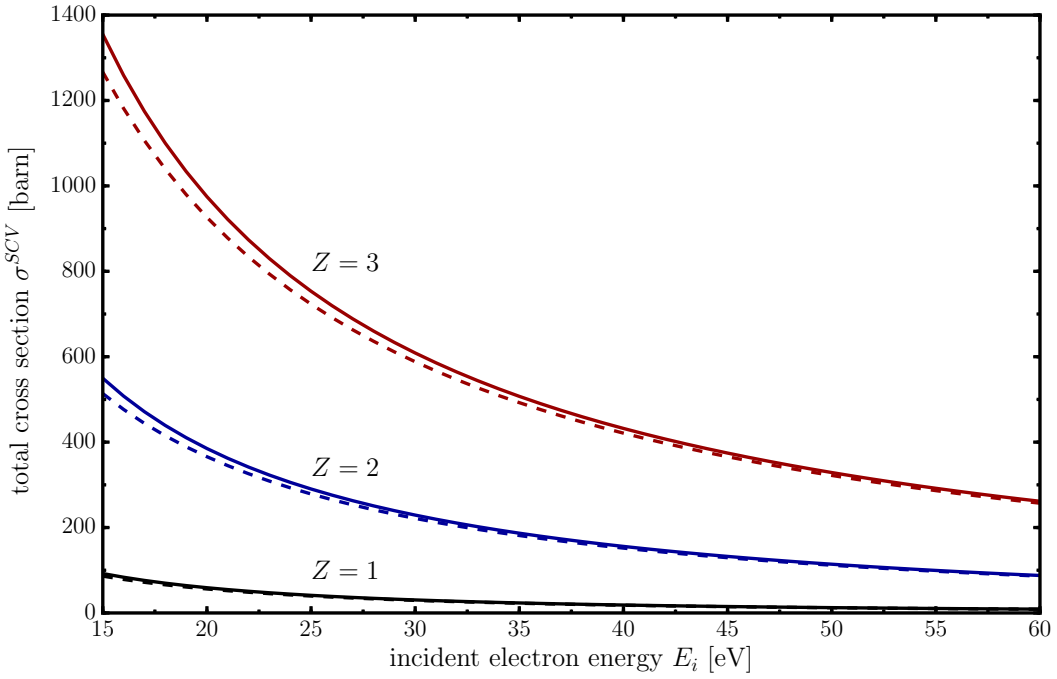

Figure 5.9: Total LARR cross section for the recombination into the ground state of a hydrogen-like ion as a function of the initial electron energy E_i. The calculations have been performed for $I_L = 10^{13}\,\mathrm{W/cm^2}$, $\omega_L = 1.17\,\mathrm{eV}$, $\theta_L = 90°$ and $\varphi_L = 0°$. We show results for three different nuclear charges $Z = 1$ (black lines), $Z = 2$ (blue lines), $Z = 3$ (red lines). For each nuclear charge we show the laser free RR result (dashed lines) and the full calculation (solid lines) in comparison.

frequency ω_L. Moreover the figure allows us to characterize the influence of the second term in the second line of Eq. (5.2), where the constituent matrix elements are "mixed". For $\theta_L = 90°$ (blue solid line) this term vanishes and the increase of the total LARR cross section compared to the laser free case is the largest. If the laser polarization is not perpendicular to the direction of the incident electron the increase of the total cross section due to the external laser is reduced. Therefore the last term in Eq. (5.2) decreases the total cross section of LARR.

Up to now we have shown that the total LARR cross section is typically increased compared to the laser free case. Moreover the results shown in Fig. 5.7 indicate that this increasement is lower if the incident electron energy is larger. In order to study this dependency of the total cross section on the incident electron energy in more detail we show in Fig. 5.9 results for σ^{SCV} (4.27) as a function of E_i again for three

different nuclear charges Z. In comparison we show results for the laser free RR cross section. For our calculations we set the laser polarization to be perpendicular to the incident electron momentum. Complied with our expectations, in Fig. 5.9 we see that the total LARR cross section decreases with increasing E_i. The difference between the total LARR cross section and the laser free result is only visible for low incident electron energies and vanishes as soon as E_i is increased.

5.2 RECOMBINATION OF VOLKOV-BESSEL ELECTRONS

All results we have shown in the previous section were obtained for electrons with a spatial structure that is asymptotically plane-wave-like. During the recent years however "twisted" electrons with a Bessel-like intensity profile and a well defined orbital angular momentum received rising interest in theory and experiment [26, 27]. Beyond the generation and characterization of such electron vortex beams nowadays sources for Bessel electrons have been developed that makes them available for experimental application [30]. Therefore first attempts have been made to theoretically investigate fundamental atomic processes with twisted electrons [35]. However the interaction of freely propagating vortex electrons with a laser field has been investigated [36], laser assisted processes with Volkov-Bessel electrons have not been addressed yet. Below we therefore will discuss results for the angle-differential partial cross section for the recombination of a Volkov-Bessel electron into the ground state of hydrogen for the case of a single atom as a target and the target averaged cross section for the case of an infinitely large target.

5.2.1 *Angular and energy distribution of the emitted photons*

The angle-differential partial cross section $\mathrm{d}\sigma_N^{VB}/\mathrm{d}\Omega_k$ (4.40) for the laser assisted recombination of a Volkov-Bessel electron into the ground state of a hydrogen atom placed in the center of the incident electron beam can be calculated by integrating the results for an incident (plane-wave-like) Volkov electron along a cone in momentum space (cf. 4.2.3). To investigate how $\mathrm{d}\sigma_N^{VB}/\mathrm{d}\Omega_k$ (4.40) depends on the opening angle θ_p and the orbital angular momentum l of the incident Volkov-Bessel electron we show $\mathrm{d}\sigma_N^{VB}/\mathrm{d}\Omega_k$ in Fig. 5.10 as a function of the recombination photon energy $\omega_k(N)$. For these calculations, we considered two values for the orbital angular momentum l and two values for the opening angle θ_p. The results are only defined at the discrete energies $\omega_k(N)$ but we show again a connecting line to guide the eye. The laser polarization is chosen perpendicular to the beam axis ($\theta_L = 90^\circ$, $\varphi_L = 0^\circ$). For this polarization of the external laser and a plane-wave-

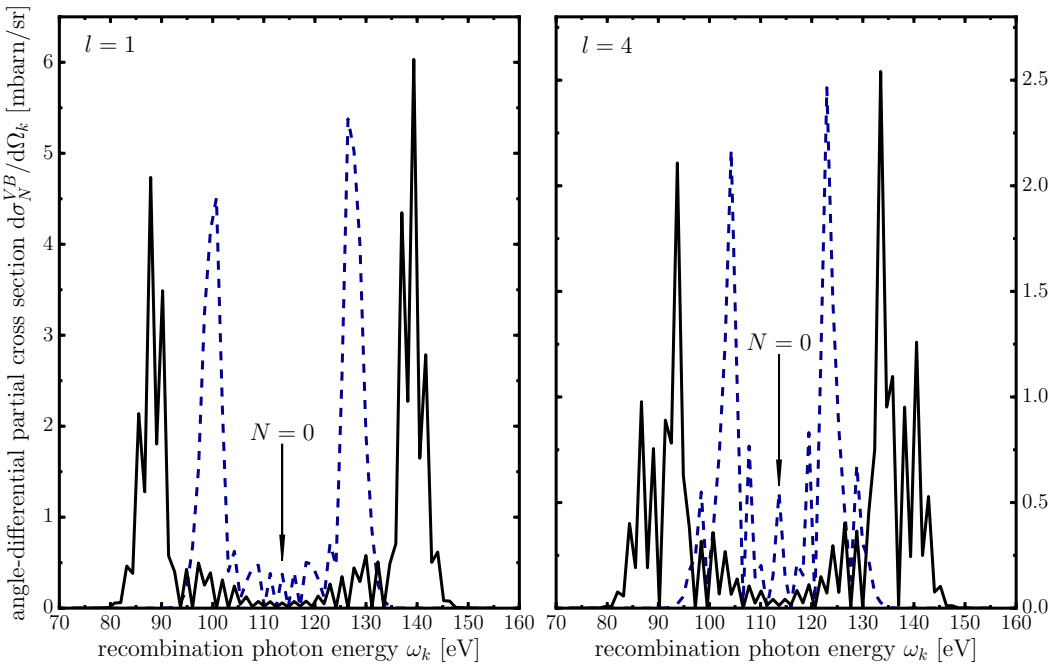

Figure 5.10: Angle-differential partial cross section for the recombination of a Volkov-Bessel electron into the ground state of hydrogen ($Z = 1$) as a function of the recombination photon energy $\hbar\omega_k(N)$. The calculations have been performed for an incident electron with energy $E_i = 100\,\mathrm{eV}$, two different opening angles $\theta_p = 45°$ (black solid line) and $\theta_p = 30°$ (blue dashed line) as well as two values for the orbital angular momentum $l = 1$ (left panel) and $l = 4$ (right panel). The external laser has an intensity of $I_L = 10^{13}\,\mathrm{W/cm^2}$ and the frequency $\omega_L = 1.17\,\mathrm{eV}$. The laser polarization is given by $\theta_L = 90°$ and $\varphi_L = 0°$ while the photon emission angle is fixed at $\theta_k = 30°$.

like incoming electron, we would expect the spectrum to be a single line, because if $\theta_L = 90°$ we have $\kappa = 0$ and therefore only the Bessel function whith $N = 0$ contributes to the angle-differential partial cross section (cf. Sec. 4.2 and Eq. (4.20)). However, due to the special spatial structure of the Volkov-Bessel electron beam more sidebands in the spectrum appear, giving it a non zero width. This width depends on the opening angle θ_p and becomes smaller, if θ_p is decreased. This can be understood by recalling that the wave function of the Volkov-Bessel electron $\widetilde{\chi}_{\boldsymbol{p}}^{VB}(\boldsymbol{r}, t)$ turns into the Volkov solution of the TDSE if $\theta_p = 0°$. Qualitatively we see that the cross section for low photon numbers N is strongly suppressed so the emitted radiation is almost two-colored. This behaviour occurs for all shown opening angles and values of the orbital angular momentum.

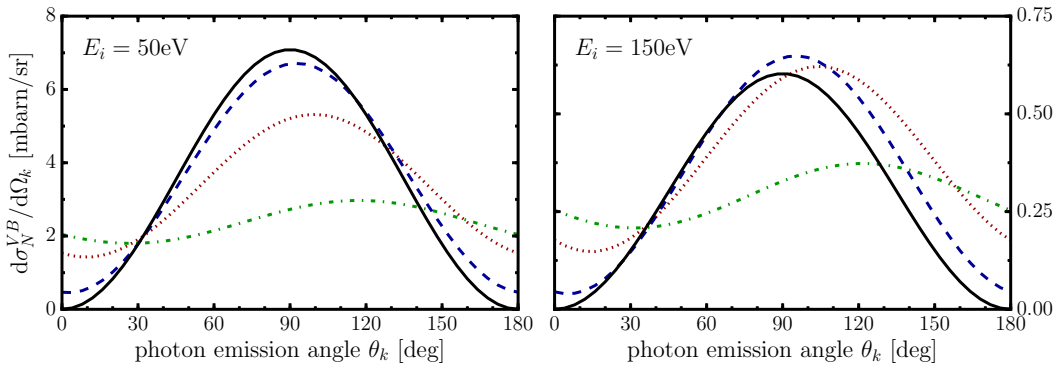

Figure 5.11: Target averaged angle-differential cross section for the recombination of a Volkov-Bessel electron into the ground state of hydrogen ($Z = 1$) as a function of the photon emission angle θ_k. The calculations have been performed for two incident electron energies $E_i = 50\,\mathrm{eV}$ (left panel) and $E_i = 150\,\mathrm{eV}$ (right panel) as well as various opening angles: $\theta_p = 1°$ (black solid lines), $\theta_p = 15°$ (blue dashed lines), $\theta_p = 30°$ (red dotted lines) and $\theta_p = 45°$ (green dash-dotted lines). The intensity of the external laser is set to $I_L = 10^{13}\,\mathrm{W/cm^2}$ and its frequency is $\omega_L = 1.17\,\mathrm{eV}$. The laser polarization is given by $\theta_L = 80°$ and $\varphi_L = 0°$ and the recombination photon is emitted under the angle $\theta_k = 30°$.

The scenario discussed above only holds for single atoms placed exactly in the center of the Volkov-Bessel electron beam. The experimental realization of this setup is nearly impossible. A more realistic scenario is the assumption of an infinitely large target and to investigate the target averaged cross section $\overline{\mathrm{d}\sigma^{VB}}/\mathrm{d}\Omega_k$. In Fig. 5.11 we show the target averaged angular distribution of the photons emitted during the laser assisted recombination of a Volkov-Bessel electron for two initial electron energies E_i and four different opening angles θ_p. To obtain the results we summed over all photon numbers N assuming that the energy of the emitted photon is not observed. In the plane wave case the angular distribution is proportional to $\sin^2\theta_k$ and therefore no photons are emitted along the z-axis. This can be seen from Eq. (4.36), where we have shown that both constituent matrix elements are proportional to $\boldsymbol{\epsilon}_k \cdot \boldsymbol{p}$, which leads to a $\sin^2\theta_k$-like angular distribution after summation over all possible polarizations $\boldsymbol{\epsilon}_k$ of the recombination photon. As we see from Fig. 5.11 the emission of photons along the propagation axis is not forbidden anymore if the incident electron beam has a non vanishing opening angle. Indeed the forward and backward emission becomes the more probable the larger θ_p becomes, while the maximum of the angular distribution is shifted towards larger photon emission angles θ_k. Similar observations have been made by Matula *et al.* [35], but they found that the maximum of the angular distribution is always

at $\theta_k = 90^\circ$. Therefore the shift of the maximum can be attributed to the external laser field. Although in all previous sections we found that the laser influence is weaker for higher incident electron energies, this is not the case for the example shown in Fig. 5.11. In fact there are no qualitative differences between the results for $E_i = 50\,\mathrm{eV}$ and for $E_i = 150\,\mathrm{eV}$.

6

SUMMARY AND OUTLOOK

In the present thesis we have performed a widespread study on laser assisted radiative recombination (LARR). For our description of LARR we have set out a theory based on the S-matrix approaches used by Shchedrin *et al.* and Li *et al.* [21, 22]. In contrast to the standard strong field approximation this approach accounts for both fields, the external laser and the Coulomb field of the nucleus, for both electron states in an approximate way. Therefore separable Coulomb-Volkov (SCV) continuum states and perturbatively dressed bound states are used for the description of the incident continuum and final bound electron, respectively.

The developed approach allowed us to perform detailed calculations for the angle-differential cross section of LARR and the spectrum, i.e. the energy distribution of the emitted recombination photons. We found that the spectrum is broadened due to the external laser field. The reason for that is the absorption or emission of laser photons by the electron which as a result may change the energy of the emitted recombination photons. The width of the broadened spectrum depends on three quantities. It is increased with increasing laser intensity I_L and incident electron energy E_i but becomes smaller if the laser frequency ω_L is enlarged. Moreover we found that the spectrum can be strongly asymmetric around the recombination photon energy that matches the energy difference between the incident electron energy and the energy of the residual bound state. We were able to find the reason for this asymmetry in the laser dressing of the final bound state. In addition we found that while in laser free radiative recombination (RR) the angular distribution of the emitted photons has a $\sin^2\theta_k$ pattern its maximum is shifted away from $\theta_k = 90^\circ$ if the process takes place in an external laser field. Similar to the spectral asymmetry this shift also origins from the bound state dressing only. Moreover it has been shown that the angular asymmetry is very sensitive to the geometry of the process, especially on the angle θ_L between the laser polarization $\boldsymbol{\epsilon}_L$ and the incident electron momentum $\boldsymbol{p}$.

Apart from the angular and energy distribution we performed calculations for the total cross section of LARR. To substantiate our numerical results we put an analytical analysis in front of these calculations. There we found that, in our model, the total cross section σ^{SCV} is influenced by the external laser only due to the dressing of the residual bound state and therefore coincides with the result for RR if the bound state dressing is neglected. The analytical formulas show that σ^{SCV}

is proportional to E_L^2/ω_L^2 and therefore scales linearly with the intensity I_L of the laser. This result is also reflected in our numerical calculations, were we moreover could show that the difference between the total cross section of LARR and RR is reduced if either the nuclear charge or the incident electron energy is increased.

In addition to our discussion of the cross section of LARR we obtained expressions for the degree of linear polarization P_{lin} and the polarization angle χ of the emitted recombination radiation. We used these expressions in order to discuss the dependence of the parameters P_{lin} and χ on the direction of the external laser polarization for the first time. While the emitted radiation is fully polarized within the xz-plane in the case of laser free RR, we found that it can depolarize to less than $P_{lin} = 0.2$ in the case of LARR if the external laser is polarized along the y-axis. As well we could show that the polarization angle χ exhibits a dependence on the energy $\omega_k(N)$ of the recombination photon that has been found similarly in the case of laser assisted Compton scattering [45].

Besides, the investigation of the laser assisted recombination of Coulomb-Volkov electrons described by SCV wave functions, we made use of the versatility of the S-matrix theory to study LARR involving twisted electrons. Therefore we had to go one step back in the adaptability of our theory, because we neglect the influence of the nucleus in our description of the incident laser driven electron vortex beam. Nevertheless, this approach is a valid approximation over a reasonable range of laser parameters, as shown by Jaroń *et al.* [19]. Within this parameter range we performed calculations for the spectrum and the angular distribution of the recombination photons emitted during the laser assisted recombination of twisted electrons and a hydrogen nucleus. We considered two different scenarios. First the collision of an electron vortex beam with a single ion placed in the center of the beam and secondly we averaged over all possible positions of the ion to describe an infinite target. In accordance with previous investigations [35, 46, 47] all dependencies on the orbital angular momentum are washed out in the latter scenario. For the non-averaged case we found that the spectrum has a two-peaked structure that is qualitatively independent on the amount of angular momentum carried by the twisted electrons. In case the initial electron state is described by a SCV wave function there are geometries under which the recombination spectrum shrinks down to a single line. In contrast to that we found for this special geometry that the energy distribution of the recombination photons has still a certain width if the incoming electron is twisted. This width exhibits a sensitivity to the opening angle of the incident electron vortex beam. While in the case of LARR involving SCV electrons the zeroes of the angular distribution of the recombination photons are only shifted due to the external laser we found that for twisted incident elec-

trons the angular distribution is always larger than zero, even if we perform the calculations for an infinite target.

Because the presented study on the laser assisted recombination of twisted electrons is the first investigation of a laser assisted atomic process involving electron vortex beams, there are several topics to be addressed beyond this thesis. Apart from the next obvious step, the calculation of the total cross section, there is a more interesting topic ahead. Because the angle-differential cross section is independent on the orbital angular momentum l of the incident twisted electrons we cannot get insight into the role this angular momentum plays in the process of LARR. One possibility to overcome this restriction is to consider neither an infinite nor a single-ion target but a target with a certain yet small extent. Currently there are works in progress on the interaction of small targets with twisted photons, indicating that such a consideration may lead to interesting results regarding the sensitivity of observable quantities with respect to l [48].

In addition to considerations involving twisted electrons that need to be laboriously prepared in experiments there are two more points worth investigating in the future. First nearly all modern experiments on the interaction of atomic systems with lasers are performed using pulsed lasers, especially in the high intensity regime. Therefore, one could search for possible effects coming from the non-infinite but pulsed external field. Secondly, there are experiments that directly measure the cross section of LARR for a final state that is not the ground state of the ion but a highly excited (Rydberg) state [8]. A direct extension of our theory to describe the recombination into such states is not possible because for these states the laser field has to be treated non-perturbatively. However there are promising approaches that could possibly be adapted to fit into the existing S-matrix framework shown in this thesis [12, 49].

Summarizing, in this thesis we have set up a theory to describe LARR in a non relativistic framework. Using this theory we obtained numerical results for the angle-differential and total cross section of the process as well as the spectrum of the recombination photons. Moreover we presented first results for the geometry- and energy dependent degree of linear polarization and polarization angle of the emitted radiation. Additionally we have performed the first study of laser assisted atomic processes involving electron vortex beams using the example of LARR. Based on the obtained results the present thesis stresses the importance of a proper description of the residual bound state and lays the foundations for further studies considering e.g. short pulses, finite targets, twisted electrons and the laser assisted recombination into highly excited states.

ACKNOWLEDGEMENTS

In the end I would like to thank all persons who have contributed to the success of this work. First of all my supervisor PD Dr. Andrey Surzhykov has to be mentioned. During the last years he gave me all the freedom and chances I could wish for while always keeping me focused on my objectives.

I have to thank Prof. Stephan Fritzsche for his support, many encouraging discussions and for his always helpful and, hence, occasionally uncomfortable questions.

With Dr. Daniel Seipt I had many discussions that were as endless as fruitful shaping new ideas for my investigations.

Finally I want to thank my parents who strongly supported me ideally as well as financially for the past five years and especially my mother who brought in her expertise to improve my English writing.

BIBLIOGRAPHY

[1] R. Schuch, T. Quinteros, M. Pajek, Y. Haruyama, H. Danared, G. Hui, G. Andler, D. Schneider, and J. Starker, Nucl. Instrum. Meth. B **79**, 59 (1993).

[2] Y. Hahn, Rep. Prog. Phys. **60**, 691 (1997).

[3] H. Yamaguchi, M. Ozawa, K. Koyama, K. Masai, J. S. Hiraga, M. Ozaki, and D. Yonetoku, Ap. J. Lett. **705**, L6 (2009).

[4] A. Surzhykov, S. Fritzsche, and T. Stöhlker, J. Phys. B **35**, 3713 (2002).

[5] S. Fritzsche, A. Surzhykov, and T. Stöhlker, Phys. Rev. A **72**, 012704 (2005).

[6] P. B. Corkum, Phys. Rev. Lett. **71**, 1994 (1993).

[7] M. Lewenstein, P. Balcou, M. Y. Ivanov, A. L'huillier, and P. B. Corkum, Phys. Rev. A **49**, 2117 (1994).

[8] M. L. Rogelstad, F. B. Yousif, T. J. Morgan, and J. B. A. Mitchell, J. Phys. B **30**, 3913 (1997).

[9] C. Wesdorp, F. Robicheaux, and L. D. Noordam, Phys. Rev. Lett. **84**, 3799 (2000).

[10] E. S. Shuman, R. R. Jones, and T. F. Gallagher, Phys. Rev. Lett. **101**, 263001 (2008).

[11] U. Schramm, J. Berger, M. Grieser, D. Habs, E. Jaeschke, G. Kilgus, D. Schwalm, A. Wolf, R. Neumann, and R. Schuch, Phys. Rev. Lett. **67**, 22 (1991).

[12] A. Scrinzi, N. Elander, and A. Wolf, Z. Phys. D **34**, 185 (1995).

[13] U. Schramm, T. Schüssler, D. Habs, D. Schwalm, and A. Wolf, Hyp. Int. **99**, 309 (1996).

[14] T. Mohamed, G. Andler, M. Fogle, E. Justiniano, S. Madzunkov, and R. Schuch, Phys. Rev. A **83**, 032702 (2011).

[15] M. Möller, Y. Cheng, S. D. Khan, B. Zhao, K. Zhao, M. Chini, G. G. Paulus, and Z. Chang, Phys. Rev. A **86**, L6 (2012).

[16] L. V. Keldysh, Sov. Phys. JETP **20**, 1307 (1965).

[17] F. H. M. Faisal, J. Phys. B **6**, L89 (1973).

[18] H. Reiss, Phys. Rev. A **22**, 1786 (1980).

[19] A. Jaroń, J. Z. Kamiński, and F. Ehlotzky, Phys. Rev. A **61**, 023404 (2000).

[20] S. Bivona, G. Bonanno, R. Burlon, and C. Leone, Phys. Rev. A **76**, 031402(R) (2007).

[21] S.-M. Li and U. D. Jentschura, J. Phys. B **42**, 185401 (2009).

[22] G. Shchedrin and A. Volberg, J. Phys. A **44**, 245301 (2011).

[23] A. N. Zheltukhin, N. L. Manakov, A. V. Flegel, and M. V. Frolov, JETP Lett. **94**, 599 (2011).

[24] A. N. Zheltukhin, A. V. Flegel, M. V. Frolov, N. L. Manakov, and A. F. Starace, J. Phys. B **45**, 081001 (2012).

[25] A. Cionga, V. Florescu, A. Maquet, and R. Taïeb, Phys. Rev. A **47**, 1830 (1993).

[26] K. Y. Bliokh, Y. P. Bliokh, S. Savel'ev, and F. Nori, Phys. Rev. Lett. **99**, 190404 (2007).

[27] M. Uchida and A. Tonomura, Nat. **464**, 737 (2010).

[28] B. J. McMorran, A. Agrawal, I. M. Anderson, A. A. Herzing, H. J. Lezec, J. J. McClelland, and J. Unguris, Science **331**, 192 (2011).

[29] J. Verbeeck, H. Tian, and P. Schattschneider, Nature **467**, 301 (2010).

[30] J. Verbeeck, H. Tian, and A. Béché, Ultramicroscopy **113**, 83 (2012).

[31] P. Schattschneider and J. Verbeeck, Ultramicroscopy **111**, 1461 (2011).

[32] M. Babiker, J. Yuan, and V. E. Lembessis, Phys. Rev. A **91**, 013806 (2015).

[33] R. van Boxem, B. Partoens, and J. Verbeeck, Phys. Rev. A **89**, 032715 (2014).

[34] V. Serbo, I. P. Ivanov, S. Fritzsche, D. Seipt, and A. Surzhykov, Phys. Rev. A **92**, 012705 (2015).

[35] O. Matula, A. G. Hayrapetyan, V. G. Serbo, A. Surzhykov, and S. Fritzsche, NJP **16**, 053024 (2014).

[36] A. G. Hayrapetyan, O. Matula, A. Aiello, A. Surzhykov, and S. Fritzsche, Phys. Rev. Lett. **112**, 134801 (2014).

[37] M. Jain and N. Tzoar, Phys. Rev. A **18**, 538 (1978).

[38] L. D. Landau and E. M. Lifshits, *Quantum mechanics: non-relativistic theory* (Butterworth-Heinemann, Oxford; Boston, 1991).

[39] P. Cavaliere, G. Ferrante, and C. Leone, J. Phys. B **13**, 4495 (1980).

[40] C. J. Joachain, N. J. Kylstra, and R. M. Potvliege, *Atoms in intense laser fields* (Cambridge University Press, Cambridge; New York, 2011).

[41] M. D. Scadron, *Advanced quantum theory and its applications through Feynman diagrams*, corr. 2. print ed., Texts and monographs in physics (Springer, New York, 1981).

[42] L. Landau, E. Lifshitz, V. Berestetski, L. Pitaevski, and J. Sykes, *Relativistic Quantum Theory*, Course of theoretical physics No. Teile 1-2 (Pergamon Press, 1971).

[43] A. I. Akhiezer and V. Berestetskii, *Quantum Electrodynamics*, 2nd ed., Interscience Monographs and Texts in Physics and Astronomy, Vol. 11 (Wiley, 1965).

[44] M. Stobbe, Ann. Phys. **399**, 661 (1930).

[45] D. Seipt and B. Kämpfer, Phys. Rev. A **89**, 023433 (2014).

[46] O. Matula, A. G. Hayrapetyan, V. G. Serbo, A. Surzhykov, and S. Fritzsche, J. Phys. B **46**, 205002 (2013).

[47] H. M. Scholz-Marggraf, S. Fritzsche, V. G. Serbo, A. Afanasev, and A. Surzhykov, Phys. Rev. A **90**, 013425 (2014).

[48] A. Surzhykov, private communication (2015).

[49] M. Klaiber and D. Dimitrovski, Phys. Rev. A **91**, 023401 (2015).

LIST OF FIGURES